Version: 02.04.2024

The Molecular Footprint of Peptides on the Surface of Ultrasmall Gold Nanoparticles (2 nm) is Governed by Steric Demand

Lisa-Sofie Wagner,[1] Oleg Prymak,[1] Torsten Schaller,[2] Christine Beuck,[3] Kateryna Loza,[1] Felix Niemeyer,[2] Nina Gumbiowski,[1] Kathrin Kostka,[1] Peter Bayer,[3] Marc Heggen,[4] Cristiano L. P. Oliveira,[5] Matthias Epple[1,*]

[1] Inorganic Chemistry and Centre for Nanointegration Duisburg-Essen (CENIDE), University of Duisburg-Essen, Universitaetsstr. 5-7, 45117 Essen, Germany

[2] Organic Chemistry, University of Duisburg-Essen, Universitaetsstr. 5-7, 45117 Essen, Germany

[3] Institute of Biology and Center for Medical Biotechnology (ZMB), University of Duisburg-Essen, Universitaetsstr. 5-7, 45117 Essen, Germany

[4] Ernst Ruska Centre for Microscopy and Spectroscopy with Electrons, Forschungszentrum Jülich, 52428 Jülich, Germany

[5] Institute of Physics, University of São Paulo, São Paulo 05508-090, Brazil

Author for correspondence: Matthias Epple, e-mail matthias.epple@uni-due.de

Abstract

Ultrasmall gold nanoparticles were functionalized with peptides of 2 to 7 amino acids that contained one cysteine molecule as anchor via a thiol-gold bond and a number of alanine residues as non-binding amino acid. The cysteine was located either in the center of the molecule or at the end (C-terminus). For comparison, gold nanoparticles were also functionalized with cysteine alone. The particles were characterized by UV spectroscopy, differential centrifugal sedimentation (DCS), high-resolution transmission electron microscopy (HRTEM), and small-angle X-ray scattering (SAXS). This confirmed the uniform metal core (2 nm diameter). The hydrodynamic diameter was probed by ^{1}H-DOSY NMR spectroscopy and showed the increase in thickness of the hydrated peptide layer with increasing peptide size (up to 1.4 nm for heptapeptides; 0.20 nm per amino acid in the peptide). ^{1}H-NMR spectroscopy on water-dispersed nanoparticles showed the integrity of the peptides and the effect of the metal

core on the peptide. Notably, the NMR signals were very broad near the metal surface and became increasingly narrow in a distance. In particular, the methyl groups of alanine can be used as probe for the resolution of the NMR spectra. The number of peptide ligands on each nanoparticle was determined by quantitative ^{1}H-NMR spectroscopy. It decreased with increasing peptide length from about 100 for a dipeptide to about 12 for a heptapeptide, resulting in an increase of the molecular footprint from about 0.1 nm^2 to 1.1 nm^2.

Keywords

Gold; nanoparticles; peptides; NMR spectroscopy; molecular footprint

Introduction

Ultrasmall gold nanoparticles have considerable potential for biomedical applications.[1-3] Due to their small size of 2 nm or less, they are able to penetrate the cell membrane and even enter the cell nucleus and cross the blood-brain barrier.[4-7] Ultrasmall nanoparticles can also be functionalized, allowing them to be used in targeted drug delivery.[8-12] Their small size allows them to make targeted interactions with biomolecules.[2] A special case are atomically sharp metal clusters for which sometimes even the crystal structure is known (see refs.[13-18] for recent comprehensive reviews). However, these are less easily prepared on a larger scale than ultrasmall nanoparticles. In turn, ultrasmall nanoparticles are less well defined and have some degree of polydispersity.[1, 2, 19]

The surface functionalization of gold nanoparticles is usually accomplished with thiol-containing ligands, which attach to the surface due to the aurophilic character of sulfur.[20-22] In addition to a direct adsorption on the gold surface, a covalent functionalization of the ligand[23-26] or a ligand exchange[27-30] are also possible. The number of ligands per nanoparticle is important to understand and to quantify the interaction of nanoparticles with targets, e.g. receptors on cells,[31, 32] or when enzymes[33, 34] or antibodies[35] are attached to a nanoparticle. Furthermore, the ligand density is important for the colloidal stability and the surface charge of the particles. However, the quantification of the ligands is sometimes difficult due to the polydispersity of the nanoparticles and the potential presence of partially unbound ligands even after purification.[36] In addition, the sensitivity of analytical methods can limit the determination of the number of ligands per nanoparticle, e.g. if a method cannot distinguish between bound and unbound ligands.[37] UV/Vis spectroscopy, fluorescence spectroscopy, elemental analysis, thermogravimetry, ICP-MS, EDX, and ^{1}H NMR spectroscopy have all been used to quantify

the ligand molecules on nanoparticles.[26, 36-42] The surface curvature plays a dominant role for the ligand density,[43, 44] clearly of high importance for ultrasmall nanoparticles.[2]

Here we demonstrate the quantification of peptides bound to ultrasmall gold nanoparticle in a comprehensive NMR study, supported by a variety of analytical methods to obtain a full characterization of the nanoparticle core with its inherent high surface curvature. We used high-resolution transmission electron microscopy (HRTEM), small-angle X-ray scattering (SAXS), differential centrifugal sedimentation (DCS), and ^{1}H-NMR diffusion-ordered spectroscopy (DOSY) as complementary methods to determine the nanoparticle size distribution. Cysteine alone and cysteine-containing peptides of different lengths were attached to the gold surface via the thiol group. Alanine was used besides cysteine because it should not interact with the gold surface. Linear peptides with a terminal cysteine and symmetric peptides with a central cysteine surrounded by alanine were used. In particular, we wanted to determine the number of ligands on each nanoparticle and their molecular footprint as a function of the length of the peptide and the position of cysteine therein.

Materials and methods

Chemicals and reagents

Tetrachloroauric acid was prepared by dissolving elemental gold (>99%) in aqua regia. Nitric acid (HNO_3, 67%), hydrochloric acid (HCl, 37%), and sodium hydroxide (NaOH, 1 M) were obtained from Bernd Kraft (Duisburg, Germany). Sodium borohydride ($NaBH_4$, >96%) and 3 kDa spin filters were obtained from Merck (Darmstadt, Germany). Maleic acid (99%) was obtained from Sigma-Aldrich (Steinheim, Germany). Deuterium oxide (D_2O, 99.9%) was obtained from Deutero GmbH (Kastellaun, Germany). L-cysteine (98%) and D-cysteine (98%) were obtained from Thermo Fisher Scientific (Schwerte, Germany). All peptides were obtained from Caslo (Kongens Lyngby, Denmark). Ultrapure water (ELGA Purelab, UK) was used for all syntheses and analyses unless otherwise stated.

Methods

The gold concentration was determined by atomic absorption spectroscopy (AAS) with a Thermo Electron M-Series spectrometer (graphite tube furnace; operated according to DIN EN ISO/IEC 17025:2005). For the measurement, 10 µL of the dispersed nanoparticles were digested with 990 µL aqua regia and diluted with 4 mL water. UV/Vis spectroscopy was performed with a Genesis 50 instrument (ThermoScientific) in quartz glass cuvettes in the range

of 200 nm to 800 nm. Differential centrifugal sedimentation (DCS) was performed with a CPS instrument DC 24000. The particles were measured at 4,000 rpm (2500 x g). A density gradient was generated with sucrose solutions (8 and 24 wt%), and 0.5 mL dodecane was used as stabilizing agent to prevent evaporation. Polyvinyl chloride particles with a defined size of 483 nm provided by CPS were used as a standard. High-resolution transmission electron microscopy (HRTEM) was performed with an aberration-corrected FEI Titan transmission electron microscope equipped with a Cs-probe corrector (CEOS Company), operating at 300 kV.[45] The images were analyzed for particle size distribution with the program ANTEMA.[46] The zeta potential of the particles was measured with a Stabino instrument (Particle Metrix). A 10 mL measuring cell with a 400 µm plunger was used. The pH was gradually reduced from 12 to 2 by adding 10 µL of 0.1 M hydrochloric acid at intervals of 10 s. For NMR spectroscopy, the dispersed nanoparticles were dispersed in 540 µL H_2O and measured after mixing with 60 µL D_2O/NaOD with water suppression at pH 12. The pure ligands were measured in D_2O with NaOD at pH 12. The ^1H NMR spectra were recorded with a Bruker Avance Neo 400 MHz and a Bruker Avance III 600 MHz spectrometer.

DOSY-NMR spectroscopy of peptide-functionalized nanoparticles dispersed in H_2O with 10% D_2O (pH 12) was performed with a Bruker Avance III 700 MHz spectrometer with a 5 mm TCI cryoprobe with a *z*-gradient at 25 °C. Presaturation for water suppression was added to a ^1H-DOSY pulse sequence from Bruker. Spectra were measured with a diffusion time of Δ = 100 ms and a pulsed gradient duration of δ = 3.5 ms for all nanoparticles. The gradient strength was incremented from 5 to 95% of the maximum gradient strength (66 G cm^{-1} for a smoothed square gradient pulse) in 32 linear steps. Spectra were processed with Topspin 3.5 (Bruker). The linearized diffusion data were plotted and fitted according to the Stejskal-Tanner equation:[47, 48]

$$\ln\left(\frac{I}{I_0}\right) = -\gamma^2 \delta^2 \left(\Delta - \delta/3\right) \cdot D \cdot G^2 \qquad (1)$$

with I = signal intensity, I_0 = signal intensity without gradient, γ = gyromagnetic ratio of ^1H, δ = diffusion gradient pulse length, Δ = diffusion delay, G = gradient strength, and D = translational diffusion coefficient. The linearized relative intensities for H_α and methyl protons of the peptide-coated nanoparticles were averaged. Error bars represent the standard deviation of these signals. While the standard error of the Stejskal-Tanner fit itself is small (<2%), we estimate the error for the diffusion coefficient to 20% due to manual integration and potentially

overlaying small signals from impurities. The hydrodynamic diameter was calculated according to the Stokes-Einstein equation:

$$d_H = \frac{k_B \cdot T}{3\pi \cdot \eta \cdot D} \quad (2)$$

with d_H = hydrodynamic diameter, k_B = Boltzmann constant, T = temperature in K, η = dynamic viscosity at 25 °C, and D = translational diffusion coefficient.

Small-angle X-ray scattering (SAXS) measurements with a scanning 1D line detector and a sample-to-detector distance of 240 mm were carried out on a laboratory Panalytical Empyrean diffractometer with Cu Kα radiation (λ = 1.54 Å, U = 40 kV and I = 40 mA) with an evacuated beam path ScatterX-78 (vacuum 0.1 mbar) in transmission mode. Colloidal dispersions of different gold nanoparticles were filled into glass capillaries (length 80 mm, outer diameter 1 mm, wall thickness 0.01 mm) and measured for 21 min with a step size of 0.01° in the 2Θ range of -0.15° to 5.00°, i.e. a q value up to 0.35 Å^{-1}. For background correction, the same capillary was filled with 0.1 M NaOH solution and measured again. The SAXS analysis was done with the Panalytical EasySAXS software 2.0 considering a polydisperse system of spheres and a desmearing effect from the line focus. The data was then fitted with the Indirect Fourier Tranformation Method (IFT),[49] where the scattering intensity $I(q)$ and the volume-weighted size distribution (D_v) assume a system of spherical homogenous particle (P_{sph}):

$$I(q) = c_v \int_0^\infty D_v(R) \cdot R^3 \cdot P_{sph}(q,R) \cdot dR \quad (3)$$

$$P_{sp}\ (q,R) = \left(3\ \frac{\sin(qR) - qR\cos(qR)}{(qR)^3}\right)^2 \quad (4)$$

with c_v a constant, q the scattering vector, defined as $q = 4\pi \sin(\Theta)/\lambda$, R and V the radius and volume of the particles, respectively.

SAXS investigations were also performed on the laboratory-based SAXS equipment Xenocs-XEUSS 2.0, located at the EMUSAXS center at the Institute of Physics, University of São Paulo, Brazil. The instrument is equipped with a Genix3D microfocus source (Cu Kα radiation, λ = 1.54 Å), a FOX3D mirror, and two sets of scatterless slits. As a result, a point-like beam with 0.7·0.7 mm^2 is obtained. The 2D scattering image was collected on a Dectris-Pilatus 300k pixel detector. The 2D images were azimuthally integrated with the program FIT2D.[50] The sample-to-detector distance was 520 mm, giving a range in q from 0.02 to 0.70 Å^{-1}. The liquid

samples (dispersions) were placed on home-made sample holders composed of borosilicate glass-capillaries with 1.5 mm diameter glued on stainless steel cases, allowing easy handling, washing and rinsing. The holders were closed with metal caps with rubber sheets. In this way, the samples could be easily placed in vacuum, allowing the measurement of the samples and buffers under exactly the same conditions. Data treatment and normalization to absolute scale were performed with the SuperSAXS Package.[51]

All particle size distributions were fitted with a Gaussian distribution which best represented the data. A log-normal distribution gave significantly worse results although it would better represent the fact that the probability for a particle diameter of zero would be zero as well.

Synthesis of gold nanoparticles

All particles were synthesized by a modified Brust-Schiffrin synthesis.[52-55] The cysteine-functionalized nanoparticles were prepared according to a modified synthesis of Ruks et al.[56] both with D- and L-cysteine. In 40 mL degassed water, tetrachloroauric acid (10 µmol, 1.97 mg gold) was dissolved. The pH was adjusted to 1.5 with about 5 mL HCl (1 M). Cysteine (3 eq., 30 µmol, 3.63 mg) was dissolved in 100 µL water and quickly added to the solution. The mixture was stirred for 10 min at room temperature, resulting in decolorization of the reaction solution. Then 200 µL of a freshly prepared sodium borohydride solution in ice-cold water (4 eq., 40 µmol, 200 mM, 7.6 g L^{-1}) was quickly added to the reaction mixture, resulting in black decolorization of the solution. The particles were isolated by centrifugation at 4000 rpm (2500 x g) for 20 min. The black precipitate was dispersed in water and centrifuged again for 20 min. The precipitated particles were redispersed in 1 M aqueous NaOH solution and stored at 4 °C.

The peptide-functionalized nanoparticles were synthesized similarly starting from tetrachloroauric acid (20 µmol, 3.94 mg Au). The corresponding peptides (3 eq., 60 µmol) were dissolved in 500 µL water and added to the tetrachloroauric acid. A decolorization of the solution was observed. Subsequently, 6.06 mg sodium borohydride (8 eq., 160 µmol) was dissolved in 800 µL ultrapure water. After rapid addition, the reaction mixture turned dark-brown. The particles were isolated by spin filtration in 3 kDa Amicon® spin filters, followed by washing with ultrapure water twelve times for 40 min each at 4000 rpm (2500 x g).

Results and discussion

All functionalized nanoparticles were prepared by a modified Brust-Schiffrin synthesis in aqueous dispersion.[55] Figure 1 shows the general reaction scheme and all peptide ligands that were used. The particles were stable under basic conditions (pH 12) but tended to agglomerate

at lower pH. Notably, the particles with shorter peptide ligands were less stable (for several hours) than those with larger peptide ligands (for several weeks).

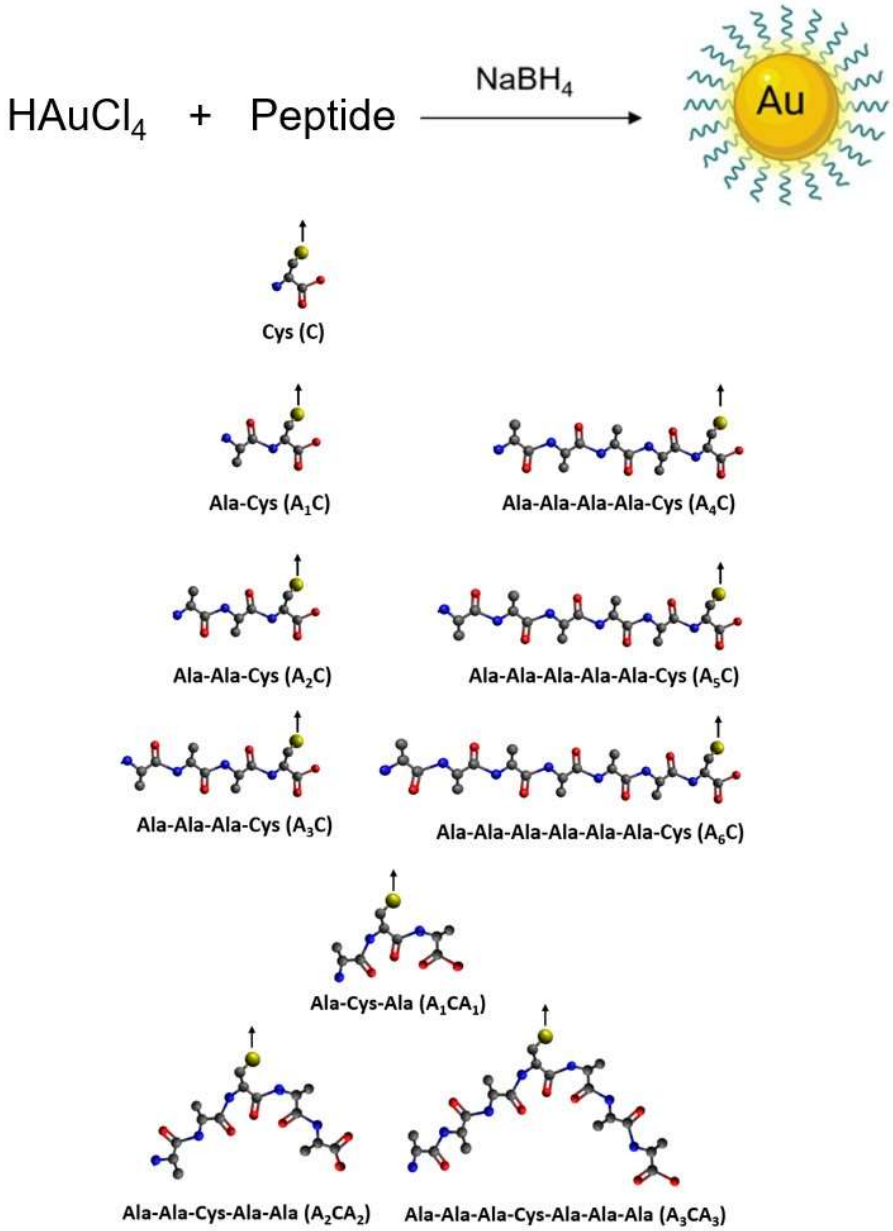

Figure 1: General reaction scheme to prepare peptide-stabilized ultrasmall gold nanoparticles (**top**) with cysteine-alanine peptides of different length (**bottom**). The arrow, originating at the cysteine thiol group, marks the attachment point of the peptide to the gold nanoparticle surface. In all peptides shown, the N-terminus is on the left and the C-terminus is on the right.

If the density of the peptide ligands on the nanoparticles shall be analyzed, it is important to have a full characterization of the metal core in terms of size and shape.[57] All nanoparticles

were comprehensively characterized by UV/Vis spectroscopy, differential centrifugal sedimentation, high-resolution transmission electron microscopy, small-angle X-ray scattering, measurement of the zeta potential, and ^{1}H-NMR spectroscopy in dispersion.

UV-Vis spectroscopy was used to exclude the presence of larger plasmonic particles that would give a surface plasmon resonance (SPR) band at about 520 nm.[58] The UV-Vis spectra (Figure 2) showed no prominent SPR band, i.e. it can be assumed that only ultrasmall nanoparticles smaller than about 3 to 4 nm were present.[26, 59, 60]

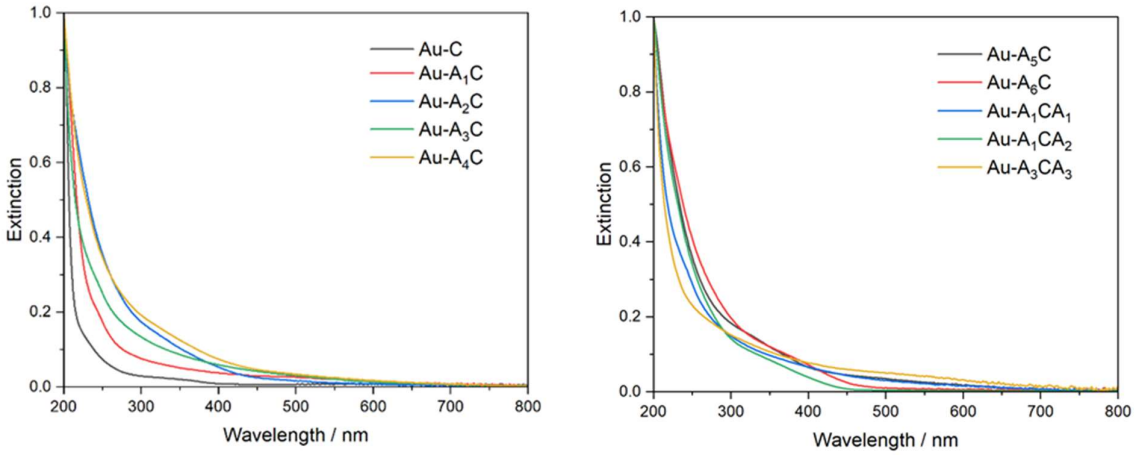

Figure 2: UV-Vis spectra of all peptide-functionalized ultrasmall gold nanoparticles dispersed in water at pH 12. Only very weak surface plasmon resonance bands around 520 nm were found in some cases as weak shoulder, indicating the absence of higher amounts of larger (plasmonic) gold nanoparticles.

The presence of ultrasmall gold nanoparticles was confirmed by differential centrifugal sedimentation (Figure 3). A monomodal particle size distribution as well as the absence of agglomeration was found for all particles with an average hydrodynamic diameter ranging from 1.30 to 1.49 nm. However, it should be noted that the size of ultrasmall nanoparticles is underestimated in DCS due to the overestimation of the effective density that is reduced by the ligand shell compared to the density of the metallic core.[61] In extreme cases, this can prevent the analysis by DCS, i.e. when a very thick ligand shell is present (demonstrated in ref.[62] for ultrasmall gold nanoparticles, functionalized with siRNA). The particles were too small to be analyzed by dynamic light scattering (DLS), underscoring the absence of larger plasmonic nanoparticles.

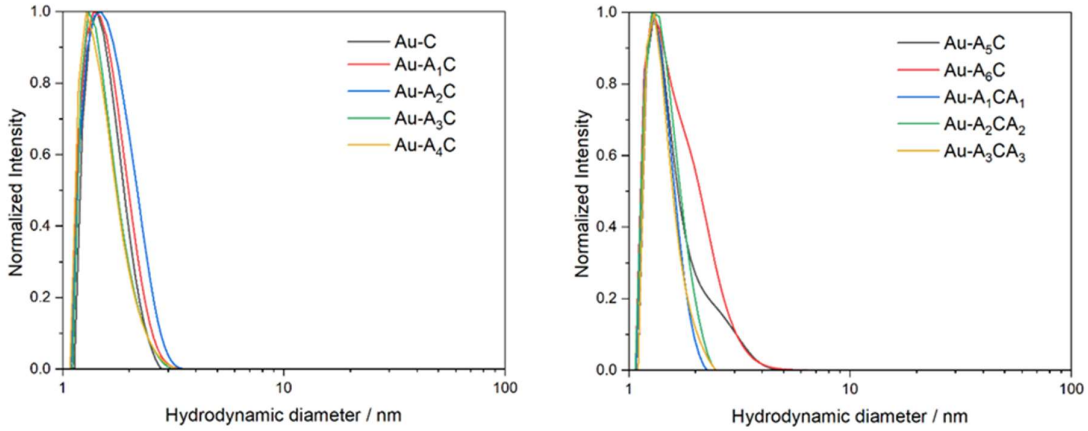

Figure 3: Differential centrifugal sedimentation of all peptide-functionalized ultrasmall gold nanoparticles, dispersed in water at pH 12. Neither larger particles nor aggregates were present, however, there is a shoulder for Au-A_5C and Au-A_6C particles which indicates a broader particle size distribution than with the other samples.

The diameter of the nanoparticle core was determined by high-resolution transmission electron microscopy. All particles had a spherical shape with an average core diameter of about 2 nm. Figure 4 shows Au-A_6C as representative example (HRTEM images of all other particles are given in the Supporting Information as Figures S1-S9).

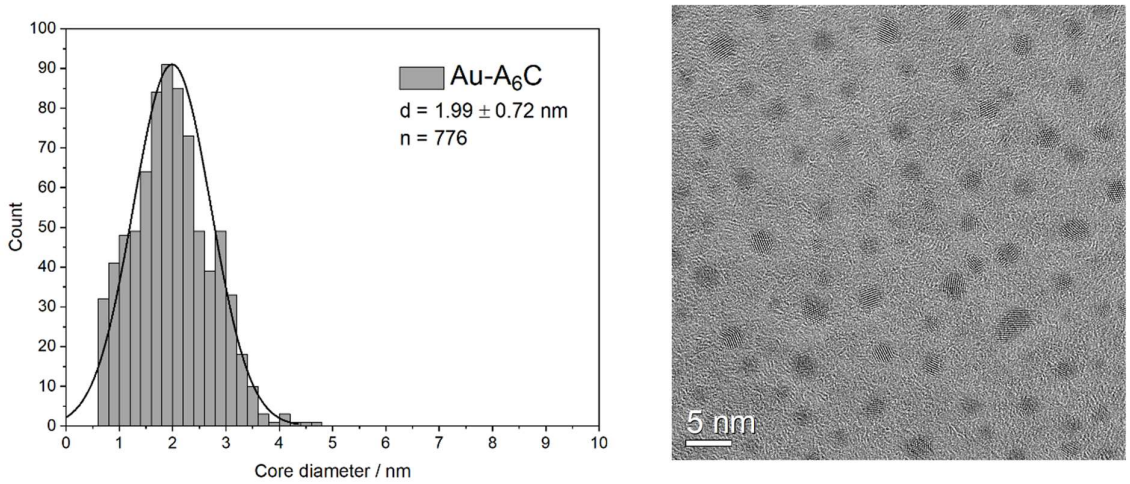

Figure 4: HRTEM images of Au-A_6C nanoparticles as representative example and its particle size distribution (gold core only). The other peptide-functionalized ultrasmall gold nanoparticles gave very similar results (see SI). The particle size distribution was determined from *n* particles (here: 776) with the program ANTEMA based on a machine learning procedure.[46]

Another method to analyze the metal core is small-angle X-ray scattering (SAXS). This was performed with water-dispersed particles (Figures 5 and S10-S18). The particles had a diameter of the metallic core $d = 2\ R_0$ between 0.9 and 2.3 nm (Table 1). The results are in good agreement with the HRTEM data. The SAXS data were fitted with the aggregated hard-spheres model[63-65]

$$I(q) = S_C \cdot S(q, R_G, Sc_{RG})_{Gui} \cdot S(q, \eta, R_{HS})_{HS} \cdot P(q, R, \sigma)_{poly} + Background \quad (5)$$

In this model, the form factor $P(q, R, \sigma)_{poly}$ describes a polydisperse system of spheres with average radius R and polydispersity σ. The polydispersity is given by a normalized Shulz-Zimm function.[66] In some cases, the formation of aggregates was observed which is expressed by the structure factor $S(q, R_G, Sc_{RG})_{Gui}$ with the overall radius of gyration R_G and the scale factor Sc_{RG}. The hard sphere interactions, described by the structure factor $S(q, \eta, R_{HS})_{HS}$ with a volume fraction η and hard sphere radius R_{HS}, account for interaction effects that cause a decrease of the scattering intensity. Interestingly, in some cases the hard sphere interactions indicated a large interaction radius with values close to the aggregate size and not to the particle size. In some cases, the fits at very low angles indicated the presence of a small fraction of even larger aggregates which would require the inclusion of a second radius of gyration in the model. This model was successfully used in our previous reports on dispersed metallic nanoparticles.[63-65] For one sample, i.e. Au-C (Figure S10), we found a broad distribution of aggregates of different size, and in this case, the Indirect Fourier Transformation (IFT) was used.

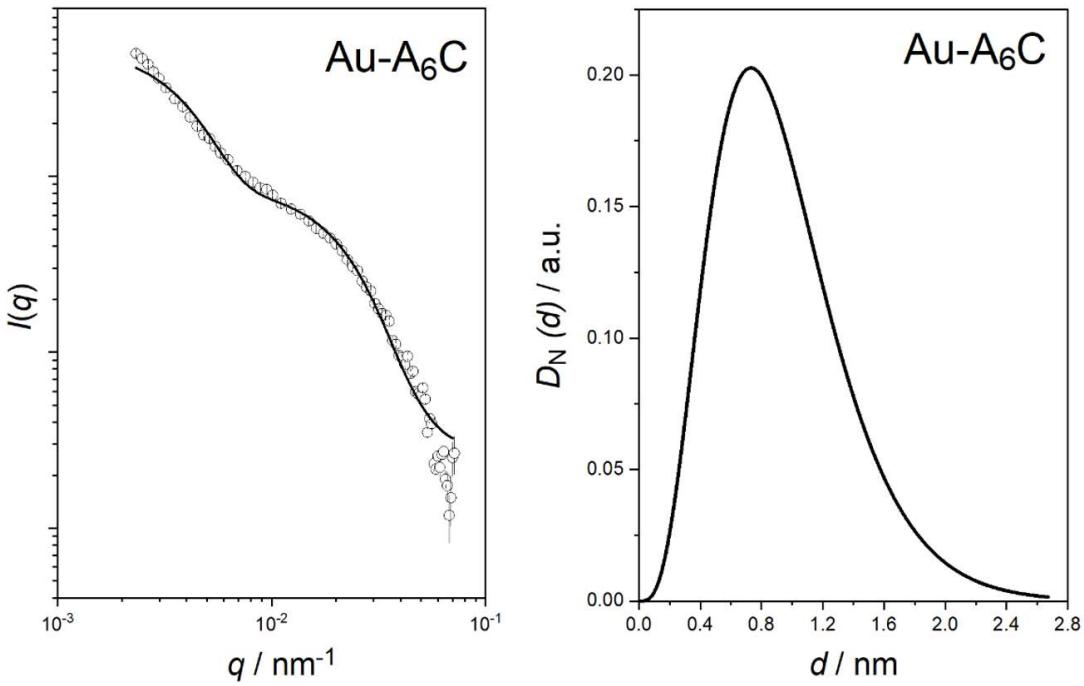

Figure 5: SAXS data of Au-A_6C nanoparticles, dispersed in water at pH 12, measured at the Xenocs-Xeuss instrument (see the SI for SAXS data of all other particle types). **Left:** Scattering curve in *q*-space. **Right:** Volume-weighted particle size distribution.

Table 1: Particle size distribution data of peptide-functionalized ultrasmall gold nanoparticles, dispersed in water (pH 12) measured by SAXS at two different instruments (Xenocs-Xeuss and Panalytical).

Nanoparticle	$d = 2 \cdot R_0$ / nm (Xenocs-Xeuss)	σ / nm (Xenocs-Xeuss)	R_G / nm (Xenocs-Xeuss)	SC_{Agg} (Xenocs-Xeuss)	$d = 2 \cdot R_0$ / nm (Panalytical)	Remarks
Au-C	2.20±0.40	1.40±0.2	-	-	-	No difference between D-cysteine and L-cysteine
Au-A_1C	1.28±0.08	0.77±0.008	2.4±0.1	0.33±0.03	2.3±0.6	-
Au-A_2C	1.40±0.20	0.86±0.08	4.1±0.1	1.40±0.10	1.3±0.5	Some agglomerates of 3.4 nm (Panalytical)
Au-A_3C	1.68±0.16	0.82±0.04	4.6±0.1	2.20±0.10	1.3±0.4	Some agglomerates of 3.8 nm (Panalytical)
Au-A_1CA_1	1.50±0.04	0.55±0.01	2.53±0.04	1.05±0.02	1.3±0.4	-
Au-A_4C	1.40±0.20	0.80±0.20	4.7±0.2	2.00±0.10	1.2±0.4	Some agglomerates of 3.1 nm (Panalytical)
Au-A_5C	1.00±0.20	0.54±0.04	2.2±0.1	1.30±0.07	1.3±0.5	-
Au-A_2CA_2	-	-	-	-	1.4±0.5	-
Au-A_6C	0.94±0.08	0.42±0.06	4.3±0.1	5.50±0.30	1.1±0.3	-
Au-A_3CA_3	-	-	-	-	1.3±0.4	-

The isoelectric point of water-dispersed nanoparticles was determined by measuring the zeta potential during a pH titration from 12 to 2 (Figure 6). All particles showed a similar trend, i.e. at basic pH, the particles had a negative zeta potential due to deprotonation of the carboxy groups. Decreasing the pH led to protonation of the carboxy and amino groups, resulting in an increase in the zeta potential. The isoelectric points of the particle species were between pH 5 and pH 6 for all particles. This agrees well with the isoelectric point of the free peptides, which are reported between pH 5 and 6,[67] indicating the integrity of the gold-bound peptides.

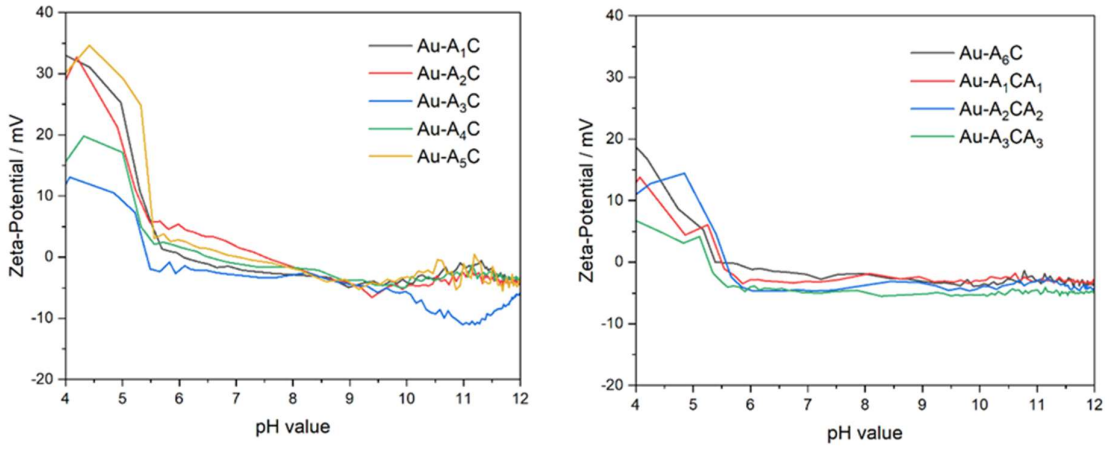

Figure 6: Zeta potential of peptide-functionalized ultrasmall gold nanoparticles dispersed in water during a titration from pH 12 to pH 2 with HCl. Below pH 4, the particles started to agglomerate and the zeta potential became unreliable (going towards zero for all particle types).

Diffusion-ordered NMR spectroscopy is a method to determine the hydrodynamic diameter of dispersed particles.[68, 69] DOSY can also distinguish between free (dissolved) ligands and surface-bound ligands. Figure 7 shows a representative Stejskal-Tanner plot for Au-A_6C nanoparticles (see Figures S19 and S20 for additional DOSY data).[48] The hydrodynamic diameters were in the range of 2 to 5 nm. Compared to the results determined by DCS, the diameters from DOSY are more reliable as this method is not based on the effective particle density,[61] but only on the mobility of the hydrated nanoparticles by diffusion. DOSY showed a clear increase of the hydrodynamic diameter with increasing length of the ligands. A linear fit gives the relationship

$$d(\text{DOSY}) / \text{nm} = (1.99 \pm 0.42) + (0.41 \pm 0.10) \cdot n \qquad (6)$$

with n the peptide length (number of amino acids). Thus, each amino acid adds about 0.20 ± 0.05 nm to the thickness of the hydrated shell. The sequence of the peptide, i.e. a terminal cysteine in comparison with a central cysteine, did not play a significant role. HRTEM and SAXS data gave the diameter of the metal core with about 2 nm, in good agreement with equation (6) which extrapolates to 1.99 ± 0.42 nm for n = 0. In order to compare size distributions as the values obtained from TEM and SAXS, the central value (average) is not sufficient because both methods give a relatively broad size distribution. In this case, the best comparison is to assess the overlap between the two size distributions by the *Z*-test:

$$Z = \frac{|d_1 - d_2|}{\sqrt{\sigma_1^2 + \sigma_1^2}}$$

where d_1 and d_2 are two central values and σ_1 and σ_2 their corresponding standard deviations. For Z between 0 and 1, the probability that the values are identical is more than 68%. As shown in Table 2, all the comparisons between HRTEM and SAXS data give Z values below 1, which indicates that the values obtained with these two techniques are statistically not different. All particle size characterization data are summarized in Table 2 and shown in Figure 8.

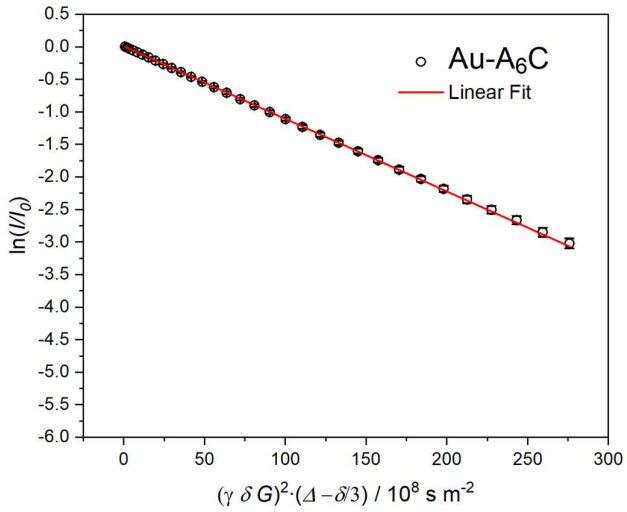

Figure 7: Representative Stejskal-Tanner plot of a ^{1}H-DOSY NMR experiment of Au-A_6C in 10% D_2O/90% H_2O (pH 12). The absolute value of the slope gives the diffusion coefficient. The corresponding Stejskal-Tanner plots of all other particles are given in Figure S19 and DOSY plots in Figure S20.

Table 2: Summary of the particle size data obtained by DCS, DOSY, HRTEM and SAXS. Errors indicate standard deviations. SAXS data labelled with an * were measured with the Panalytical instrument. All other SAXS data were measured with the Xenoc-Xeuss instrument.

Nanoparticle	Hydro-dynamic diameter by DCS / nm	Hydro-dynamic diameter by ^{1}H DOSY / nm	Core diameter by HRTEM / nm	Core diameter by SAXS / nm	$Z_{HRTEM-SAXS}$
Au-C	1.46 ± 0.37	2.08 ± 0.42	1.94 ± 0.63	2.20 ±1.40	0.17
Au-A_1C	1.47 ± 0.45	3.07 ± 0.61	2.07 ± 0.79	1.28 ± 0.77	0.72
Au-A_2C	1.49 ± 0.43	3.60 ± 0.72	2.09 ± 0.64	1.40 ± 0.86	0.64
Au-A_3C	1.31 ± 0.24	3.80 ± 0.76	2.15 ± 0.62	1.68 ± 0.82	0.46
Au-A_1CA_1	1.30 ± 0.18	3.69 ± 0.74	2.16 ± 0.63	1.50 ± 0.55	0.79
Au-A_4C	1.30 ± 0.22	4.00 ± 0.80	1.85 ± 0.67	1.40 ± 0.80	0.43
Au-A_5C	1.30 ± 0.26	3.77 ± 0.75	1.82 ± 0.71	1.00 ± 0.60	0.88
Au-A_2CA_2	1.39 ± 0.23	4.73 ± 0.95	2.27 ± 0.76	1.4 ± 0.5 *	0.96
Au-A_6C	1.30 ± 0.40	4.43 ± 0.89	1.99 ± 0.72	0.94 ± 0.40	0.83
Au-A_3CA_3	1.30 ± 0.16	5.08 ± 1.02	1.90 ± 0.60	1.3 ± 0.4 *	0.17

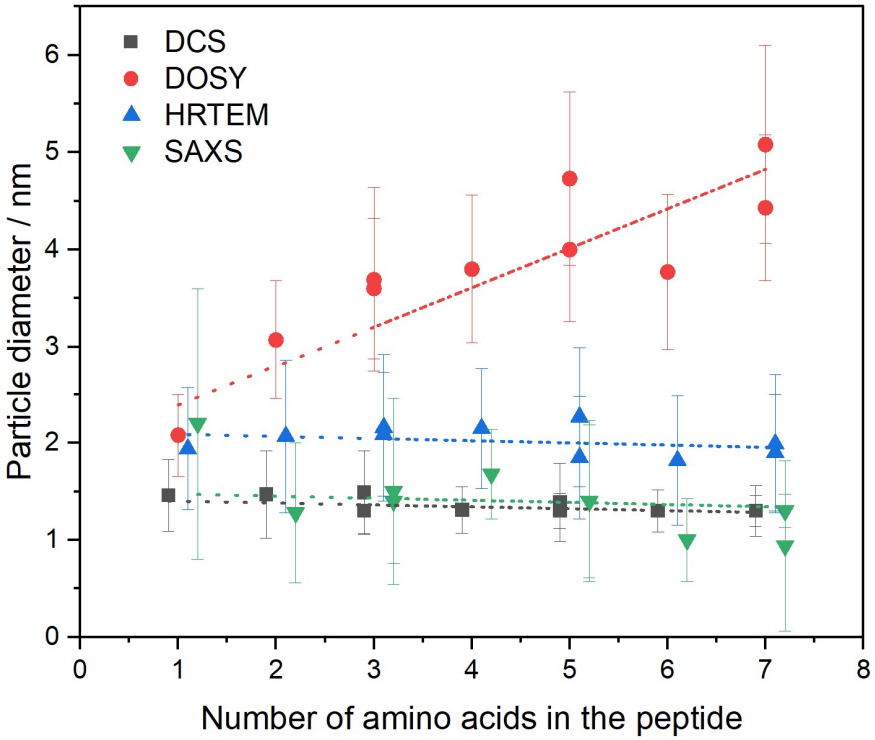

Figure 8: Particle diameter as determined by different methods. The particle diameter is shown as a function of the peptide length. TEM and SAXS show the diameter of the metallic core whereas DOSY probes the hydrodynamic diameter that includes the hydrated peptide shell.

DCS also probes the hydrodynamic diameter but gives diameters that are consistently too small for ultrasmall nanoparticles.[61]

Surface properties and successful surface functionalization of ultrasmall gold nanoparticles can be investigated by NMR spectroscopy, in contrast to larger nanoparticles where the resolution is limited due to very broad or even absent NMR signals.[26, 68, 70, 71] Indeed, NMR spectroscopy, also multidimensional, has been used to elucidate the ligand nature in atom-sharp gold clusters like $Au_{102}(pMBA)_{44}$ (pMBA: para-mercaptobenzoic acid)[72] and $Au_{144}(SR)_{60}$ (R=Et, Pr).[73] NMR spectroscopy can also be used to determine the number of ligands per nanoparticle. Figure 9 shows a representative ^1H NMR spectrum of the ligand A_2C and the nanoparticle Au-A_2C. The mobility of the bound ligands is decreased due to the close proximity to the metal core, resulting in a shortened spin-spin relaxation time.[70] As a consequence, the signals of the bound ligands showed an increased peak width compared to the free ligands. In addition, a characteristic downfield shift of the signals to higher frequencies was observed.[26, 71]

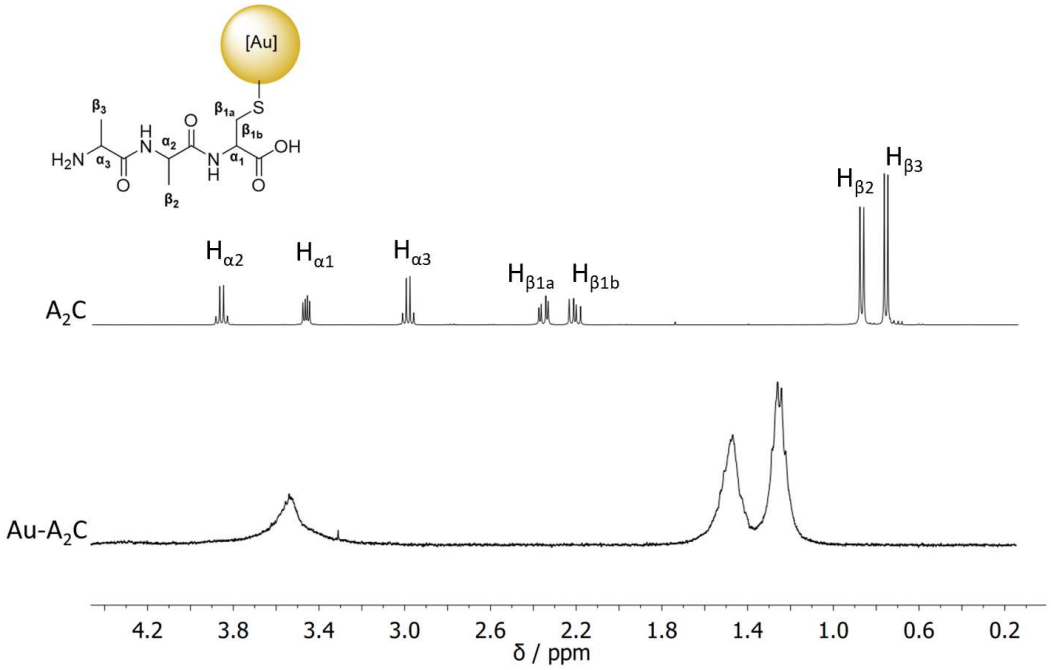

Figure 9: Representative ^1H NMR spectra of the ligand A_2C (**top**) and the coated nanoparticle Au-A_2C (**bottom**) in 10% D_2O/90% H_2O (pH 12). NMR spectra of all other peptides and peptide-conjugated nanoparticles are given in Figures S21 to S29.

The ^{1}H NMR spectra of ultrasmall gold nanoparticles functionalized with peptides showed broader peaks compared to the spectra of the free ligands (Figure 10 and Figures S21 to S29). All ligands were bound to the nanoparticles as there were no sharp peaks of dissolved (free) ligands.[74] In general, the binding of the ligands to the nanoparticle particularly affected the signals of protons close to the nucleus, such as $H_{\beta 1a}$ and $H_{\beta 1b}$ of cysteine,[26, 75] with decreasing shifts for protons farther away from the metal surface. Note that due to the suppression of water at 4.79 ppm, the neighboring NMR signals were partially suppressed as well, i.e. the integrals were smaller than expected. For particles functionalized with the dipeptide A_1C, two broad signals were found. The first signal was assigned to the methyl group of alanine (1.3 ppm) and the second to the methine protons of alanine (3.6 ppm). For longer peptides, multiple signals between 1.20 and 1.60 ppm were found, belonging to the methyl groups of the outer and inner alanine residues in the peptide sequence.

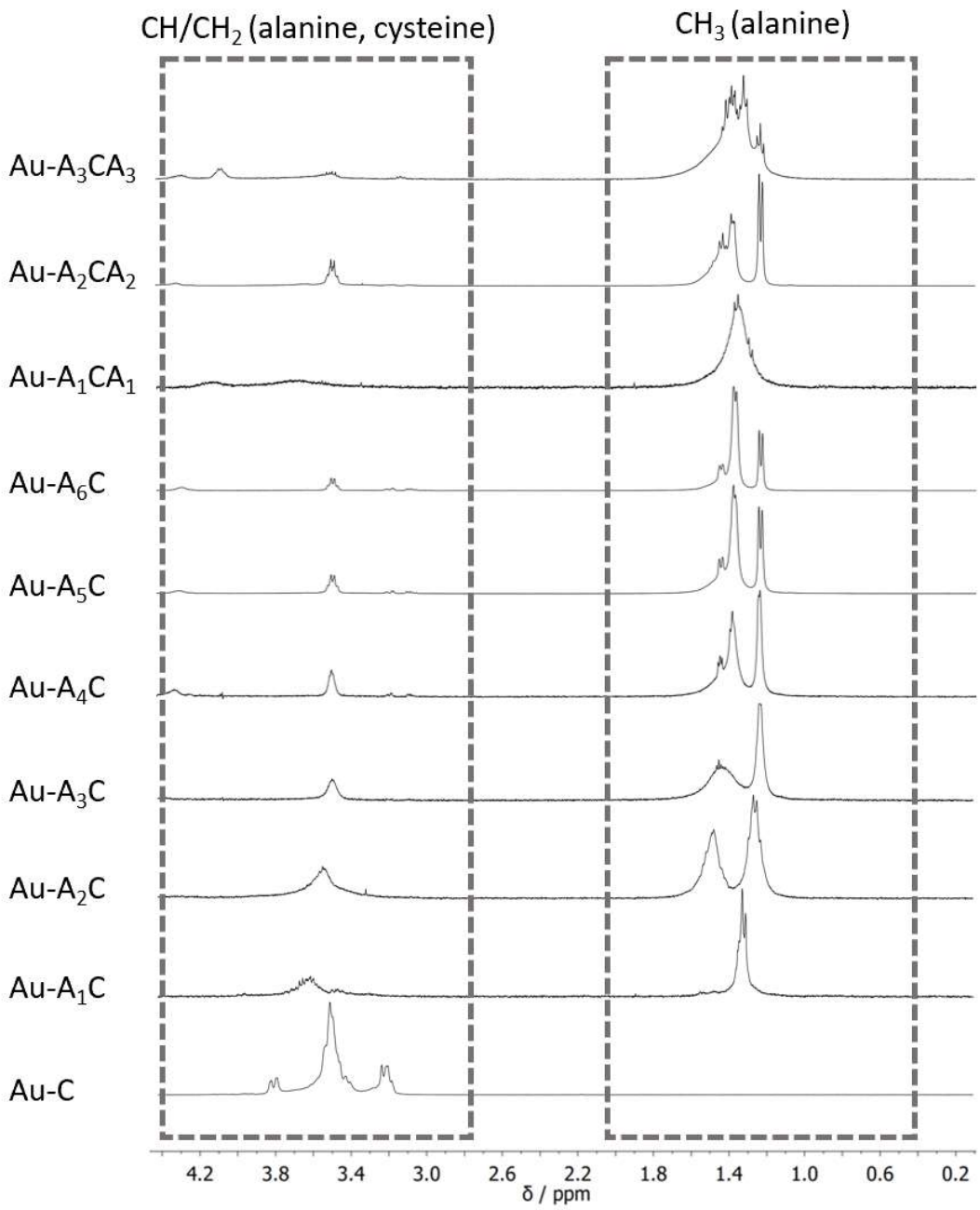

Figure 10: ^{1}H NMR spectra of peptide-functionalized ultrasmall gold nanoparticles dispersed in 10% D_2O/90% H_2O (pH 12). A characteristic signal broadening due to the vicinity of the metal surface can be seen. The major regions where sets of NMR peaks occur are enclosed in boxes.

The protons of the H_α groups of the alanine residues were present in the range between 3.20 to 4.00 ppm for all particles. Signals of the methyl protons, especially of the methyl group of the outer alanines, became narrower with increasing length of the peptide due to their increased

flexibility/range of motion. Figure 11 shows a magnification of this spectral range. At very high distance to the metal core, these groups increasingly resembled the sharp signals of the free peptides, despite the downfield shifts. If we take the hydrodynamic diameter as probed by DOSY, it can be assumed that the distance between the farthest amino acids and the metal surface is about 1 to 1.5 nm for longer peptides.

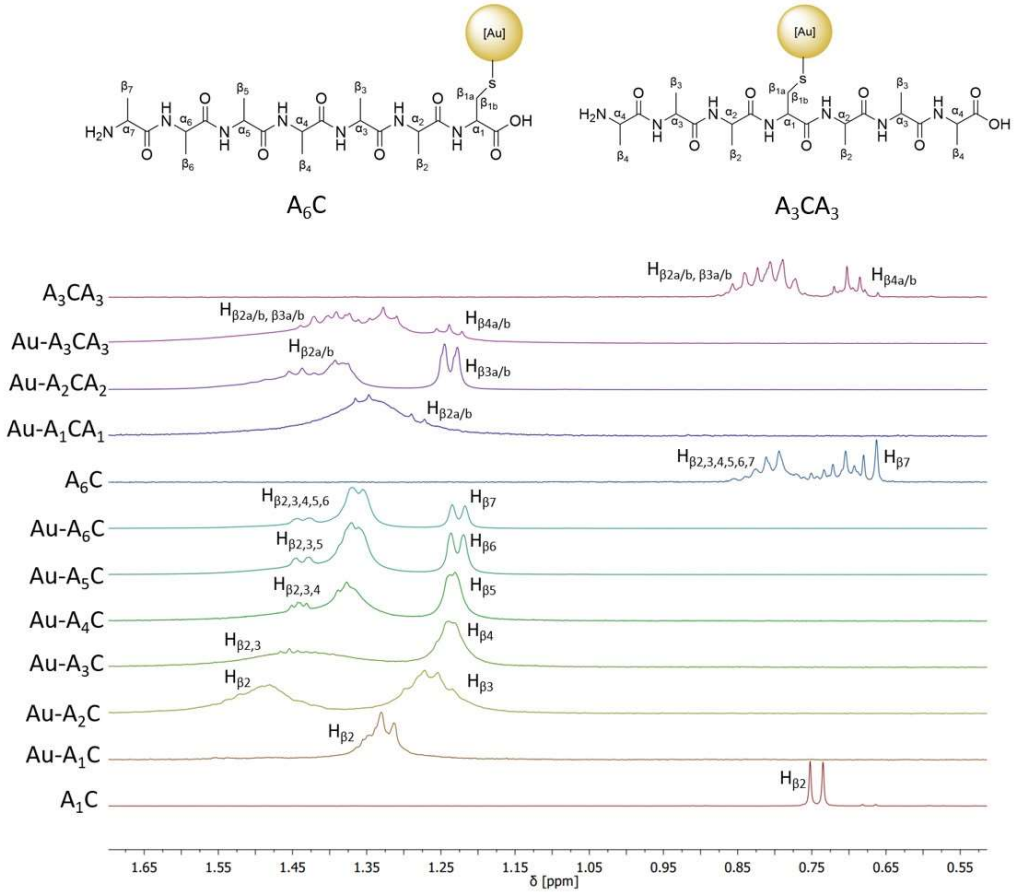

Figure 11: Magnification of the ^{1}H NMR spectra of peptide-functionalized ultrasmall gold nanoparticles dispersed in 10% D_2O/90% H_2O (pH 12). The region of the methyl groups of alanine is shown. The spectra of the dissolved peptides A_1C, A_6C, and A_3CA_3 are shown for comparison.

The number of ligands on each nanoparticle was quantified by ^{1}H NMR spectroscopy. Maleic acid was used as an internal calibration standard (Figure 12). The ligand concentration can be determined from the relative integrals of the protons and the known concentration of maleic acid.

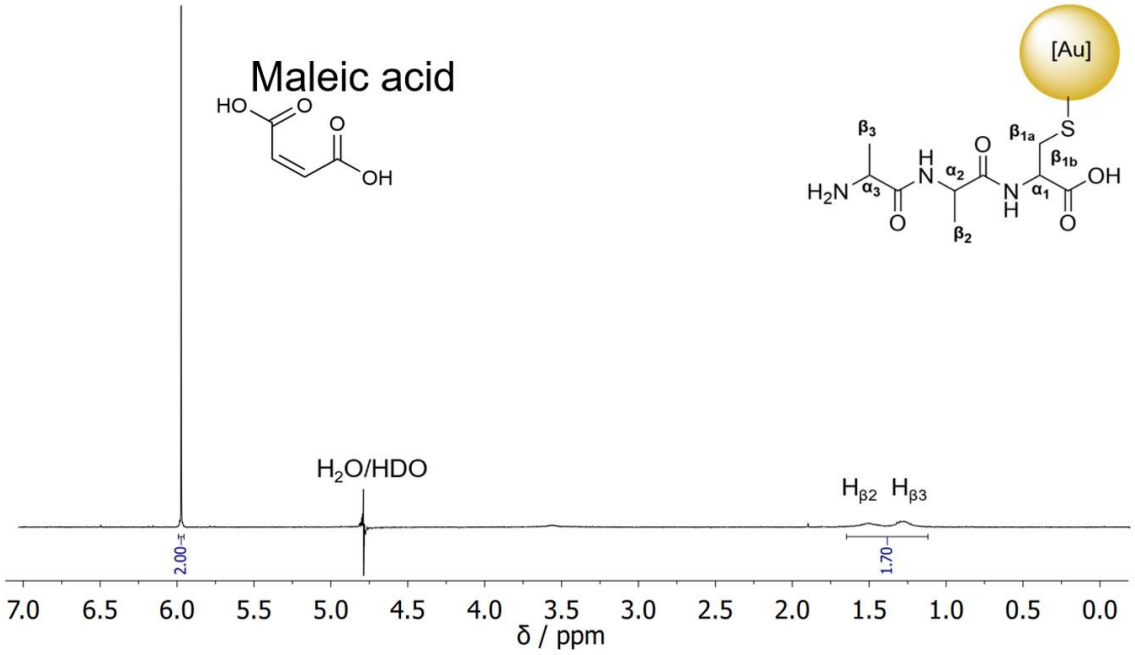

Figure 12: ^{1}H NMR spectrum of the Au-A_2C nanoparticles functionalized with the tripeptide A_2C in the presence of maleic acid as internal standard, dissolved in D_2O at pH 12. The ligand concentration was determined by integration of the peak of maleic acid and the peaks of the methyl groups of the ligands ($H_{\beta2}$, $H_{\beta3}$).

The nanoparticle concentration was obtained from the gold concentration, determined by atomic absorption spectroscopy (AAS), assuming spherical particles with an average diameter of 2 nm (see ref. [26] for details of a full computation). The number of gold atoms in a spherical particle with 2 nm diameter is about 250.[76] The ratio of the molar concentrations of ligands and particles gives the number of ligands per particle. If a spherical particle with a diameter of 2 nm is assumed (average of HRTEM and SAXS results; Table 2), its surface area is 12.6 nm^2. This area permits to compute the molecular footprint of each ligand on the nanoparticle surface.[26] We set the average particle diameter to 2 nm for all particle types because the differences among them were statistically insignificant. Assuming a variable particle diameter (e.g. the average diameter from Table 2) would change the number of ligands on each nanoparticle considerably and make a comparison difficult. Together with the fact that the particles were not strictly spherical, this approach appears reasonable to discuss the ligand number on the particles as a function of ligand type.

The number of ligands on each nanoparticle decreased with increasing ligand size, i.e. peptide length. In turn, the molecular footprint of each ligand peptide increased. Figure 13 shows the

number of ligands per nanoparticle and the molecular footprint. For Au-A_6C, only 13 ligands were bound to each particle, in contrast to 175 cysteine molecules for Au-C. As a result, the molecular footprint increased from 0.07 nm^2 for Au-C to 0.97 nm^2 for Au-A_6C. Surprisingly, there was no significant difference between linear peptides with a terminal cysteine and branched peptides of the same length with a central cysteine. Importantly, there is no indication from NMR spectroscopy that the ligands are bound in two or more layers as this would immediately show up in the NMR spectra as a second set of sharper peaks. Furthermore, the bond between ligand and particle is very stable as no free (=desorbed and dissolved) ligands were found in the NMR spectra. Thus, we can assume a monolayer of peptide molecules on the nanoparticle surface.

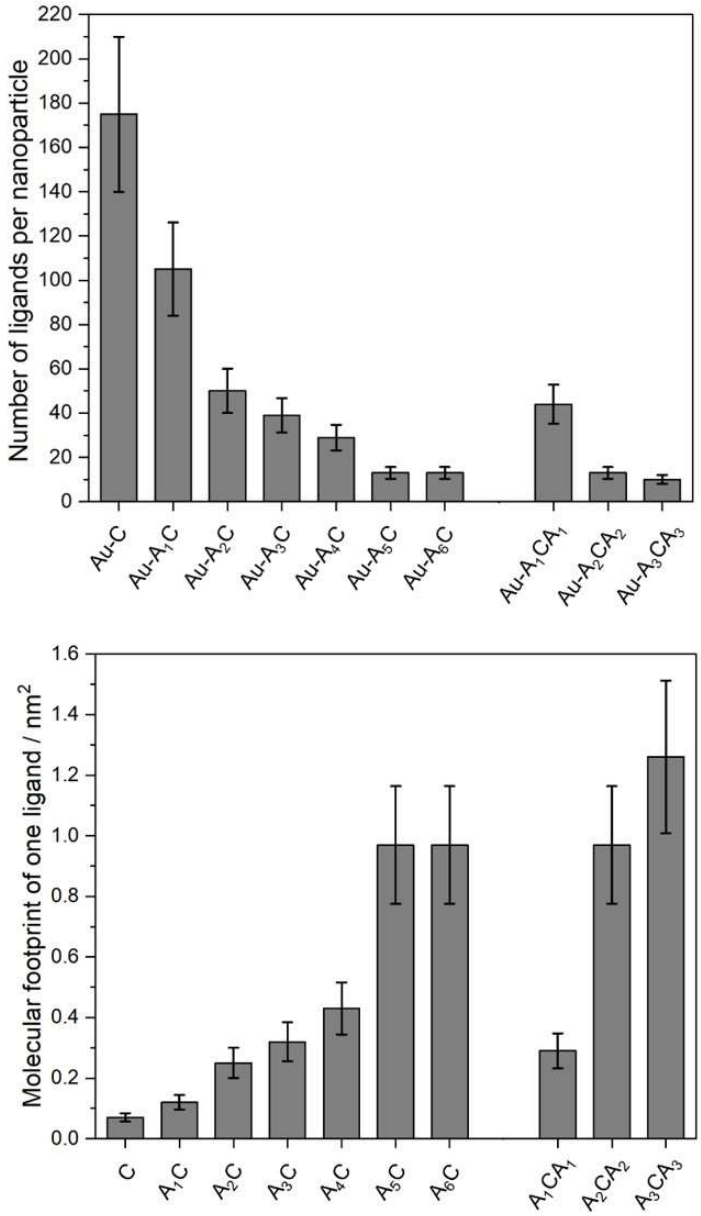

Figure 13: Number of peptide ligands on each gold nanoparticle (core diameter: 2 nm) (**top**) and molecular footprint of each peptide ligand (**bottom**). With increasing peptide length, the number of ligands per nanoparticle decreases and the molecular footprint increases. The accuracy of the method is estimated to ±20% as indicated by error bars.

The increasing molecular footprint with increasing peptide length is ascribed to steric interaction between the ligands, i.e. it indicates a close packing on the particle surface. This effect has been reported earlier in the literature for gold nanoparticles. Hinterwirth et al. observed a decrease in ligand number with increasing ligand length by ICP-MS with ω-mercaptoalkanoic acids and mercapto-poly(ethylene glycol) carboxylic acids. The molecular

footprint was in a similar range with 0.16-0.23 nm^2.[36] Rahme et al. analyzed gold nanoparticles with a diameter of 15 nm functionalized with thiolated polyethylene glycol by thermogravimetry. They showed a decrease in ligand density with an increase in steric demand.[77] Picardi et al. demonstrated that a copper complex with a disulfide ligand (lipoic acid) can bind to the surface of 40 nm gold nanoparticles with a molecular footprint of 0.71 nm^2.[78] Ming et al. found a molecular footprint of 0.24 nm^2 for pyrene-carrying thioesters and thiocarbonates on 12.5 nm gold particles.[79] Ruks et al. synthesized cysteine-functionalized ultrasmall gold nanoparticles. They determined a molecular footprint of 0.19 nm^2.[74] For ultrasmall gold nanoparticles functionalized with a fluorescence-labeled hexapeptide, they found a footprint per ligand of 0.10 nm^2.[56] Van der Meer et al. found molecular footprints in the range of 0.15 to 0.40 nm^2 for each cysteine linker of a precision macromolecule that was attached to ultrasmall gold particles (2 nm) via cysteine.[80] Klein et al. determined a molecular footprint of the tripeptide glutathione (GSH) of 0.10 nm^2 on 2 nm gold nanoparticles.[26] It is remarkable that the footprints determined here for the tripeptides A_2C (0.25 nm^2) and A_1CA_1 (0.29 nm^2) were significantly higher. It was shown by Wolff et al.[71] and Wetzel et al.[81] for ultrasmall silver and platinum nanoparticles that the footprint of glutathione also depended on the core metal of the nanoparticles. Karki et al. used NMR spectroscopy and DFT calculations to investigate how the peptides Ala-Ala-Cys and the reverse variant attach to gold nanoparticles via the thiol group. The decisive factor here was whether the amino group or the carboxylate group was in the vicinity of the sulfur. This had a considerable influence on the structure of the peptide-gold system. With Cys-Ala-Ala, a monolayer was formed parallel to the gold surface, while Ala-Ala-Cys tended to form a bilayer.[82]

Turning to the effect of curvature (as defined by the particle size), Jimenez et al. considered the molecular footprint of hexanethiol on gold nanoparticles of different size in a molecular dynamics (MD) study. They found a molecular footprint of 0.21 nm^2 on a flat gold surface with a steep decrease for smaller particles (4.4 nm diameter: 0.14 nm^2; 2 nm diameter: 0.12 nm^2).[43] In experiments on SAMs on planar gold surfaces, n-alkylthiols adsorbed on (111) and (100) single-crystal gold substrates were examined. The density of the thiols on the surface was limited by steric effects, as in our study, giving typical molecular footprints of 0.22 nm^2.[83, 84] This was confirmed by Chavez et al. who performed electrochemical measurements of thiolated polyethylene glycols on planar gold surfaces and found a molecular footprint of 0.29 to 0.44 nm^2, increasing with the length of the polyethylene glycol chain.[85] Wu et al. discussed the influence of the ligand density as a function of the size of the nanoparticles. They investigated gold nanospheres with diameters from 1.2 to 25 nm that were functionalized with

(mercaptohexadecyl)trimethylammonium bromide (MTAB). They showed that the ligand density decreased with increasing nanoparticle size. For large nanoparticles with a diameter of 25 nm, 3 molecules per nm^2 were found, while the number increased to 5-6 for 10 nm particles. They established by NMR studies and MD simulations that it is not the sulfur packing on the nanoparticle surface that limits the ligand density, but rather the packing of head group that carries the thiol. While the ligands were more ordered on larger nanoparticles, the ligands were less ordered and more mobile on small nanoparticles, induced by the high curvature. Ligand islands were also present, which led to tighter packing of the head groups between the neighboring ligands.[86]

Murray et al. discussed alkylthiolate monolayers as a function of the gold core size. Gold clusters with a diameter of 1.5 to 5.2 nm were prepared and functionalized with dodecanethiol. They studied the monolayer coverage, examining the transition from a 2D self-assembled monolayer (SAM) to a 3D SAM. For larger clusters, the radius of curvature was significantly higher, resulting in a layer resembling a 2D SAM. Smaller clusters were more likely to form a 3D SAM, which led to a higher number of surface defect locations and a decreased radius of curvature. These defects led to an increased surface density.[87-89] The decreased molecular footprint on nanoparticles with high surface curvature was also postulated by Rahnamoun et al. for poly(oxonorbornenes).[90] Localized surface plasmon resonance spectroscopy (LSPRS) was used by Lanterna et al. to investigate gold nanoparticles functionalized with heterocyclic sulfur-containing compounds. It was shown that the surface loading depended on both the molecular geometry of the ligands and the size (i.e. curvature) of the nanoparticles. The density of the ligands remained almost constant with increasing nanoparticle diameter, while the number of ligands increased with increasing ligand length at the same size, in good agreement with our results.[91] Table 3 summarizes molecular footprint data of the particles studied here and from the literature. As the effects of ligand size and particle size (curvature) are clearly overlapping, the trend of ligand density is difficult to assess. Nevertheless, a comparison is possible for gold nanoparticles of the same size.

Generally, it can be stated that the density of the ligands on the surface of ultrasmall gold nanoparticles is very high. For di- or tripeptides, the number of ligands is about half of the number of gold atoms (about 250). Stoichiometries of gold clusters with peptides were determined at the end of the 1990s by mass spectrometry, usually after gel electrophoretic separation. Glutathione which binds via a central cysteine turned out to be an especially useful ligand. In 1998, Whetten et al. isolated a glutathione-coated gold cluster with the composition $Au_{28}(GSH)_{16}$.[39, 40] In 2004, Negishi et al. identified the following compositions for glutathione-

covered gold clusters by mass spectrometry: $Au_{18}(GSH)_{11}Cl_x$, $Au_{21}(GSH)_{12}Cl_x$, $Au_{28}(GSH)_{16}Cl_x$, $Au_{32}(GSH)_{18}Cl_x$, and $Au_{39}(GSH)_{23}Cl_x$.[41] In 2005, this was revised and extended to $Au_{10}(GSH)_{10}$, $Au_{15}(GSH)_{13}$, $Au_{18}(GSH)_{14}$, $Au_{22}(GSH)_{16}$, $Au_{22}(GSH)_{17}$, $Au_{25}(GSH)_{18}$, $Au_{29}(GSH)_{20}$, $Au_{33}(GSH)_{22}$, and $Au_{39}(GSH)_{24}$.[42] The particle size was 1 nm or less. If we tentatively assume a diameter of 1 nm, the surface area per cluster is about 3.1 nm^2, leading to molecular footprints of about 3.1 / 20 = 0.155 nm^2, well in line with the ultrasmall nanoparticles studied here.

It also compares well with atom-sharp clusters where the number of ligands is about 30-60% of the number of metal atoms due to the high surface curvature and the high number of metal atoms on the particle surface,[14] e.g. $Au_{32}(R_3P)_{12}Cl_8$ (R=Et, ^{n}Pr, ^{n}Bu),[92] $Au_{102}(pMBA)_{44}$ (pMBA: para-mercaptobenzoic acid),[93, 94] and $Au_{144}(SR)_{60}$.[73] For atom-sharp clusters with thiolate ligands, Dass gave the relationship[44]

$$\text{ligand number} = 10.46 + 0.33 \cdot \text{number of gold atoms} \quad (7)$$

For a 2 nm gold particle with 250 gold atoms, this gives 92 ligands and a molecular footprint of 0.14 nm^2, in good agreement with the binding of short peptides studied here.

Notably, the conjugation of larger ligands to a glutathione-azide-terminated gold surface via click chemistry (CuAAC) leads to fewer ligands with a higher molecular footprint. This was found for 2 nm gold nanoparticles carrying Cy3 molecules (5 per nanoparticle, 2.5 nm^2 each),[4] Cy5 molecules (36 per nanoparticle; 0.35 nm^2 each),[95] FAM molecules (6 per nanoparticle, 2.1 nm^2 each),[26, 96] AlexaFluor-647 molecules (11 to 18 per nanoparticle, 0.70 to 1.15 nm^2 each),[26, 95] nanobodies (5 per nanoparticle, 2.5 nm^2 each),[97] siRNA molecules (6 to 10 per nanoparticle, 1.4 to 2.0 nm^2 each),[62] or molecular tweezers (11 to 30 per nanoparticle, 0.42 to 1.14 nm^2 each).[25] A quantitative assessment of the clicking efficiency on glutathione-azide-terminated 2 nm gold nanoparticles showed that only 6 to 11 out of 118 available azide groups were used for conjugation.[26] Clearly, larger molecules and longer peptides need more space on the nanoparticle surface, i.e. they cannot use all potential conjugation sites for clicking. Similarly, Ha et al. found a molecular footprint of 2.3 nm^2 for phosphine-bound calix[8]arene ligands on 4 nm gold nanoparticles.[98] Rai et al. attached the antimicrobial peptide cecropin-melittin (16 amino acids) to the surface of 14 nm nanoparticles. Here, 240 peptides were bound on each nanoparticle with a considerably high molecular footprint of 2.57 nm^2.[99] This compares well to the size of the largest peptides used here (n=7), i.e. it confirms that the number of ligands is governed by steric demand.

Finally, it must be mentioned that the presence of the peptides during the reduction of gold may already influence the gold core. In principle, it would be possible to prepare standard particles of the same size (e.g. with glutathione as ligand) and then exchange glutathione by the peptides used here during immersion.[28, 30, 37, 100, 101] In that case, one would have to prove that the ligand exchange was complete and that the gold core was not influenced by the exchange reaction (e.g. by surface etching with peptide ligands). Therefore, we believe that this alternative synthetic pathway would give rise to even more significant concerns than the method we employed. Note that the results presented and discussed here are focused on ultrasmall metal nanoparticles of approximately spherical shape. The situation will change with other particle cores (like quantum dots) or other geometries like nanorods. However, Fisher et al. estimated 65 stearic acid ligands (C_{18}) on a 3 nm CdSe quantum dot with a molecular footprint of 0.44 nm^2, i.e. a similar as in the case of ultrasmall metallic nanoparticles.[102]

Table 3: Molecular footprint of various compounds on the surface of metallic nanoparticles of different size. AA: Number of amino acids in a peptide. Usually, spherical particles have been assumed for the computations.

Core metal	Ligand	Number of amino acids	Particle core diameter / nm	Experimental methods	Number of ligands per particle	Molecular footprint of each ligand / nm^2	Reference
Au	C (cysteine)	1	2	^{1}H-NMR	175	0.07	This work
Au	cysteine	1	1.78	^{13}C-NMR	67	0.15	Ruks et al.[74]
Au	A_1C	2	2	^{1}H-NMR	105	0.12	This work
Au	A_2C	3	2	^{1}H-NMR	50	0.25	This work
Au	A_1CA_1	3	2	^{1}H-NMR	44	0.29	This work
Au	GSH	3	2	^{1}H-NMR	125	0.10	Klein et al.[26]
Ag	GSH	3	2	^{1}H-NMR, ICP-MS	171	0.073	Wolff et al.[71]
Ag	GSH	3	2	^{1}H-NMR	150 to 160	0.08	Wetzel et al.[103]
AgPt	GSH	3	2	^{1}H-NMR, ICP-MS	336	0.037	Wolff et al.[71]
Pt	GSH	3	2	^{1}H-NMR, ICP-MS	313	0.040	Wolff et al.[71]
Au	GSH	3	2	^{1}H-NMR, ICP-MS	169	0.074	Wolff et al.[71]
Au	A_3C	4	2	^{1}H-NMR	39	0.32	This work
Au	A_4C	5	2	^{1}H-NMR	29	0.43	This work
Au	A_2CA_2	5	2	^{1}H-NMR	13	0.97	This work
Au	A_5C	6	2	^{1}H-NMR	13	0.97	This work
Au	A_6C	7	2	^{1}H-NMR	13	0.97	This work
Au	A_3CA_3	7	2	^{1}H-NMR	10	1.26	This work
Au	peptides	6 to 9	2	^{1}H-NMR, UV-vis	129 to 176	0.07 to 0.1	Ruks et al.[56]
Au	cecropin-melittin (16 AA)	16	14	spectrophotometry	240	2.57	Rai et al.[99]
Au	CRaf (36 AA)	36	1.55	UV-vis	18	0.41	Ruks et al.[104]
Au	PEG_7, PEG_4, MHA, MUA, MPA		13.2 to 26.2	ICP-MS	4.3-6.3 ligands nm^{-2}	0.16 to 0.23	Hinterwirth et al.[26]
Au	MTAB		1.2 to 25	^{1}H-NMR, UV-vis	2-6 ligands nm^{-2}	0.17 to 0.5	Wu et al.[86]
Au	alkanethiols		1.5 to 5.2	FT-IR, DSC, TGA, XPS	53 to 520	0.13 to 0.16	Hostetler et al.[88]
Au	citrate		13	TGA and CHNS analysis	3.1	0.32	Rostek et al.[105]
Au	oligo(amidoamine)s		2	^{1}H-NMR	36-99	0.15-0.40 per cysteine	van der Meer et al.[80]
Au	3*H*-1,2-dithiole-3-thiones		7, 25, 49	LSPR, SERS, NMR	1.2 to 5 ligands/nm^2	0.2 to 0.83	Lanterna et al.[91]
Au	pyrene-carrying thioesters		12.5	fluorescence spectroscopy	2000	0.24	Ming et al.[79]
Au	Cu complex bound via lipoic acid		40	ICP-AES	7000	0.71	Picardi et al. [78]

Conclusions

Gold nanoparticles functionalized with peptides of different lengths were synthesized and characterized. Various methods were used to analyze the ultrasmall nanoparticles. The particles had an average diameter of the metal core of 2 nm as shown by HRTEM and SAXS which probe the metal core of hundreds of particles in the dried state (HRTEM) and of millions of particles in dispersion (SAXS). Thus, they look on the particles in different states, giving a comprehensive view of the metal core. DCS systematically underestimates the particle diameter due to the effective particle density that is lowered by the hydrated peptide shell, but it shows a good dispersibility of the nanoparticles. ^{1}H-DOSY NMR spectroscopy, looking on the conjugated ligand shell only, gave reliable hydrodynamic particle diameters that permitted to estimate the thickness of the hydrated peptide shell (up to 1.5 nm for a heptapeptide). The attached peptides showed the same protonation behavior as the dissolved peptides as indicated by the zeta potential as a function of pH. The successful surface functionalization was assessed by ^{1}H NMR spectroscopy which was well applicable to ultrasmall particles. Binding to the nanoparticle was evident by a downfield shift as well as a broadening of the signals. The ligand density as determined by ^{1}H-NMR spectroscopy decreased with increasing peptide length, resulting in an increase of the molecular footprint. This is probably due to increased steric demand and hindrance, although the high curvature of ultrasmall nanoparticles enabled a higher ligand density compared to larger nanoparticles. There was no significant difference between peptides of the same length (3, 5, 7) bound with a terminal cysteine and peptides bound with a central cysteine. This suggests a disordered state of the peptide on the nanoparticle surface, i.e. a not an ordered brush-like conformation. Of course, the molecular footprint depends on the nature of the ligand and also on the dispersion medium during synthesis. Finally, the dispersion medium (here: water) will determine the solvation of the ligand shell during the synthesis and thereby the steric demand.

Conflicts of Interest

The authors declare no conflict of interest.

Acknowledgments

M.E. and M.H. are grateful to the Deutsche Forschungsgemeinschaft (DFG) for funding in the projects EP 22/62-1 and HE 7192/8-1. M.E. and C.L.P.O. are grateful to the German Academic Exchange Service (DAAD) and Fundação Coordenação de Aperfeiçoamento de Pessoal de Nível Superior (CAPES, Finance Code 001) for funding of a joint project in the framework of

PROBRAL/PPP. This study was financed in part by the Coordenação de Aperfeiçoamento de Pessoal de Nível Superior - Brasil (CAPES), Finance Code 001. C.L.P.O is supported by São Paulo Research Foundation (FAPESP) grant #2016/24531-3, Conselho Nacional de Desenvolvimento Científico e Tecnológico (CNPq) grant #303001/2019-4, and INCT-FCx (Instituto Nacional de Ciência e Tecnologia de Fluidos Complexos). We thank Beate Römer and Robin Meya for elemental analyses and the EMUSAXS technicians Igino Martins and Gabriel B. M. Teobaldo for support with the SAXS data acquisition.

Supplementary Material

The supplementary material shows HRTEM images and particle size distributions of all particles, ^{1}H-NMR spectra of all particles and dissolved peptides, ^{1}H-DOSY NMR data of all particles, and SAXS data of all particles.

References

(1) Zarschler, K.; Rocks, L.; Licciardello, N.; Boselli, L.; Polo, E.; Garcia, K. P.; De Cola, L.; Stephan, H.; Dawson, K. A. Ultrasmall inorganic nanoparticles: State-of-the-art and perspectives for biomedical applications. *Nanomedicine* **2016**, *12*, 1663-1701.

(2) Epple, M.; Rotello, V. M.; Dawson, K. The why and how of ultrasmall nanoparticles. *Acc. Chem. Res.* **2023**, *56*, 3369-3378.

(3) Huang, R.; Luther, D. C.; Zhang, X.; Gupta, A.; Tufts, S. A.; Rotello, V. M. Engineering the interface between inorganic nanoparticles and biological systems through ligand design. *Nanomaterials* **2021**, *11*, 1001.

(4) Sokolova, V.; Nzou, G.; van der Meer, S. B.; Ruks, T.; Heggen, M.; Loza, K.; Hagemann, N.; Murke, F.; Giebel, B.; Hermann, D. M.; et al. Ultrasmall gold nanoparticles (2 nm) can penetrate and enter cell nuclei in an in-vitro brain spheroid model. *Acta Biomater.* **2020**, *111*, 349-362.

(5) Sokolova, V.; Mekky, G.; van der Meer, S. B.; Seeds, M. C.; Atala, A. J.; Epple, M. Transport of ultrasmall gold nanoparticles (2 nm) across the blood-brain barrier in a six-cell brain spheroid model. *Sci. Rep.* **2020**, *10*, 18033.

(6) Huo, S.; Jin, S.; Ma, X.; Xue, X.; Yang, K.; Kumar, A.; Wang, P. C.; Zhang, J.; Hu, Z.; Liang, X. J. Ultrasmall gold nanoparticles as carriers for nucleus-based gene therapy due to size-dependent nuclear entry. *ACS Nano* **2014**, *8*, 5852-5862.

(7) Huang, K.; Ma, H.; Liu, J.; Huo, S.; Kumar, A.; Wei, T.; Zhang, X.; Jin, S.; Gan, Y.; Wang, P. C.; et al. Size-dependent localization and penetration of ultrasmall gold nanoparticles in cancer cells, multicellular spheroids, and tumors in vivo. *ACS Nano* **2012**, *6*, 4483-4493.

(8) Fan, M.; Han, Y.; Gao, S. T.; Yan, H. Y.; Cao, L. Z.; Li, Z. H.; Liang, X. J.; Zhang, J. C. Ultrasmall gold nanoparticles in cancer diagnosis and therapy. *Theranostics* **2020**, *10*, 4944-4957.

(9) Kluenker, M.; Mondeshki, M.; Tahir, M. N.; Tremel, W. Monitoring thiol-ligand exchange on Au nanoparticle surfaces. *Langmuir* **2018**, *34*, 1700-1710.

(10) Kopp, M.; Kollenda, S.; Epple, M. Nanoparticle–protein interactions: Therapeutic approaches and supramolecular chemistry. *Acc. Chem. Res.* **2017**, *50*, 1383-1390.

(11) Luther, D. C.; Huang, R.; Jeon, T.; Zhang, X. Z.; Lee, Y. W.; Nagaraj, H.; Rotello, V. M. Delivery of drugs, proteins, and nucleic acids using inorganic nanoparticles. *Adv. Drug Deliv. Rev.* **2020**, *156*, 188-213.
(12) Pelaz, B.; Alexiou, C.; Alvarez-Puebla, R. A.; Alves, F.; Andrews, A. M.; Ashraf, S.; Balogh, L. P.; Ballerini, L.; Bestetti, A.; Brendel, C.; et al. Diverse applications of nanomedicine. *ACS Nano* **2017**, *11*, 2313-2381.
(13) Antoine, R.; Broyer, M.; Dugourd, P. Metal nanoclusters: from fundamental aspects to electronic properties and optical applications. *Sci. Technol. Adv. Mater.* **2023**, *24*, 2222546.
(14) Kang, X.; Li, Y. W.; Zhu, M. Z.; Jin, R. C. Atomically precise alloy nanoclusters: Syntheses, structures, and properties. *Chem. Soc. Rev.* **2020**, *49*, 6443-6514.
(15) Yang, J.; Jin, R. C. New advances in atomically precise silver nanoclusters. *ACS Mater. Lett.* **2019**, *1*, 482-489.
(16) Zeng, C. J. Precision at the nanoscale: On the structure and property evolution of gold nanoclusters. *Pure Appl. Chem.* **2018**, *90*, 1409-1427.
(17) Zaleska-Medynska, A.; Marchelek, M.; Diak, M.; Grabowska, E. Noble metal-based bimetallic nanoparticles: the effect of the structure on the optical, catalytic and photocatalytic properties. *Adv. Colloid Interface Sci.* **2016**, *229*, 80-107.
(18) Jin, R.; Zeng, C.; Zhou, M.; Chen, Y. Atomically precise colloidal metal nanoclusters and nanoparticles: fundamentals and opportunities. *Chem. Rev.* **2016**, *116*, 10346-10413.
(19) Tang, J.; Shi, H. H.; Ma, G. Y.; Luo, L. P.; Tang, Z. H. Ultrasmall Au and Ag nanoclusters for biomedical applications: A review. *Front. Bioeng. Biotechnol.* **2020**, *8*, 1019.
(20) Inkpen, M. S.; Liu, Z. F.; Li, H.; Campos, L. M.; Neaton, J. B.; Venkataraman, L. Non-chemisorbed gold-sulfur binding prevails in self-assembled monolayers. *Nat. Chem.* **2019**, *11*, 351-358.
(21) Reimers, J. R.; Ford, M. J.; Marcuccio, S. M.; Ulstrup, J.; Hush, N. S. Competition of van der Waals and chemical forces on gold–sulfur surfaces and nanoparticles. *Nat. Rev. Chem.* **2017**, *1*, 0017.
(22) Häkkinen, H. The gold–sulfur interface at the nanoscale. *Nat. Chem.* **2012**, *4*, 443-455.
(23) Sander, F.; Fluch, U.; Hermes, J. P.; Mayor, M. Dumbbells, trikes and quads: Organic-inorganic hybrid nanoarchitectures based on "clicked" gold nanoparticles. *Small* **2014**, *10*, 349-359.
(24) Rana, S.; Yeh, Y. C.; Rotello, V. M. Engineering the nanoparticle-protein interface: applications and possibilities. *Curr. Opin. Cell Biol.* **2010**, *14*, 828-834.
(25) van der Meer, S. B.; Hadrovic, I.; Meiners, A.; Loza, K.; Heggen, M.; Knauer, S. K.; Bayer, P.; Schrader, T.; Beuck, C.; Epple, M. New tools to probe the protein surface: ultrasmall gold nanoparticles carry amino acid binders. *J. Phys. Chem. B* **2021**, *125*, 115-127.
(26) Klein, K.; Loza, K.; Heggen, M.; Epple, M. An efficient method for covalent surface functionalization of ultrasmall metallic nanoparticles by surface azidation, followed by copper-catalyzed azide-alkyne cycloaddition. *ChemNanoMat* **2021**, *7*, 1330-1339.
(27) Woehrle, G. H.; Brown, L. O.; Hutchison, J. E. Thiol-functionalized, 1.5-nm gold nanoparticles through ligand exchange reactions: scope and mechanism of ligand exchange. *J. Am. Chem. Soc.* **2005**, *127*, 2172-2183.
(28) Zan, X. F.; Li, Q. Z.; Pan, Y. T.; Morris, D. J.; Zhang, P.; Li, P.; Yu, H. Z.; Zhu, M. Z. Versatile ligand-exchange method for the synthesis of water-soluble monodisperse AuAg nanoclusters for cancer therapy. *ACS Appl. Nano Mater.* **2018**, *1*, 6773-6781.
(29) Chen, Y. P.; Xianyu, Y. L.; Jiang, X. Y. Surface modification of gold nanoparticles with small molecules for biochemical analysis. *Acc. Chem. Res.* **2017**, *50*, 310-319.
(30) Dinkel, R.; Braunschweig, B.; Peukert, W. Fast and slow ligand exchange at the surface of colloidal gold nanoparticles. *J. Phys. Chem. C* **2016**, *120*, 1673-1682.
(31) Lee, H.; Odom, T. W. Controlling ligand density on nanoparticles as a means to enhance biological activity. *Nanomedicine* **2015**, *10*, 177-180.

(32) Su, G.; Jiang, H.; Xu, B.; Yu, Y.; Chen, X. Effects of protein corona on active and passive targeting of cyclic RGD peptide-functionalized PEGylation nanoparticles. *Mol. Pharmaceut.* **2018**, *15*, 5019-5030.
(33) Bortot, A.; Zanzoni, S.; D'Onofrio, M.; Assfalg, M. Specific interaction sites determine differential adsorption of protein structural isomers on nanoparticle surfaces. *Chem. Eur. J.* **2018**, *24*, 5911-5919.
(34) Wang, Y. M.; Jonkute, R.; Lindmark, H.; Keighron, J. D.; Cans, A. S. Molecular crowding and a minimal footprint at a gold nanoparticle support stabilize glucose oxidase and boost its activity. *Langmuir* **2020**, *36*, 37-46.
(35) Ma, L. L.; Tam, J. O.; Willsey, B. W.; Rigdon, D.; Ramesh, R.; Sokolov, K.; Johnston, K. P. Selective targeting of antibody conjugated multifunctional nanoclusters (nanoroses) to epidermal growth factor receptors in cancer cells. *Langmuir* **2011**, *27*, 7681-7690.
(36) Hinterwirth, H.; Kappel, S.; Waitz, T.; Prohaska, T.; Lindner, W.; Lämmerhofer, M. Quantifying thiol ligand density of self-assembled monolayers on gold nanoparticles by inductively coupled plasma-mass spectrometry. *ACS Nano* **2013**, *7*, 1129-1136.
(37) Smith, A. M.; Marbella, L. E.; Johnston, K. A.; Hartmann, M. J.; Crawford, S. E.; Kozycz, L. M.; Seferos, D. S.; Millstone, J. E. Quantitative analysis of thiolated ligand exchange on gold nanoparticles monitored by ^{1}H NMR spectroscopy. *Anal. Chem.* **2015**, *87*, 2771-2778.
(38) Mullen, D. G.; Fang, M.; Desai, A.; Baker, J. R.; Orr, B. G.; Holl, M. M. B. A quantitative assessment of nanoparticle−ligand distributions: implications for targeted drug and imaging delivery in dendrimer conjugates. *ACS Nano* **2010**, *4*, 657-670.
(39) Schaaff, T. G.; Knight, G.; Shafigullin, M. N.; Borkman, R. F.; Whetten, R. L. Isolation and selected properties of a 10.4 kDa gold:glutathione cluster compound. *J. Phys. Chem. B* **1998**, *102*, 10643-10646.
(40) Schaaff, T. G.; Whetten, R. L. Giant gold−glutathione cluster compounds: Intense optical activity in metal-based transitions. *J. Phys. Chem. B* **2000**, *104*, 2630-2641.
(41) Negishi, Y.; Takasugi, Y.; Sato, S.; Yao, H.; Kimura, K.; Tsukuda, T. Magic-numbered Au(n) clusters protected by glutathione monolayers (n = 18, 21, 25, 28, 32, 39): Isolation and spectroscopic characterization. *J. Am. Chem. Soc.* **2004**, *126*, 6518-6519.
(42) Negishi, Y.; Nobusada, K.; Tsukuda, T. Glutathione-protected gold clusters revisited: Bridging the gap between gold(I)−thiolate complexes and thiolate-protected gold nanocrystals. *J. Am. Chem. Soc.* **2005**, *127*, 5261-5270.
(43) Jimenez, A.; Sarsa, A.; Blazquez, M.; Pineda, T. A molecular dynamics study of the surfactant surface density of alkanethiol self-assembled monolayers on gold nanoparticles as a function of the radius. *J. Phys. Chem. C* **2010**, *114*, 21309-21314.
(44) Dass, A. Mass spectrometric identification of Au68(SR)34 molecular gold nanoclusters with 34-electron shell closing. *J. Am. Chem. Soc.* **2009**, *131*, 11666-11667.
(45) Barthel, J.; Houben, L.; Tillmann, K. FEI Titan G3 50-300 PICO. *J. Large-scale Res. Fac.* **2015**, *1*, A34.
(46) Gumbiowski, N.; Loza, K.; Heggen, M.; Epple, M. Automated analysis of transmission electron micrographs of metallic nanoparticles by machine learning. *Nanoscale Adv.* **2023**, *5*, 2318-2326.
(47) Altieri, A. S.; Hinton, D. P.; Byrd, R. A. Association of biomolecular systems via pulsed-field gradient NMR self-diffusion measurements. *J. Am. Chem. Soc.* **1995**, *117*, 7566-7567.
(48) Stejskal, E. O.; Tanner, J. E. Spin diffusion measurements: Spin echoes in the presence of a time-dependent field gradient. *J. Chem. Phys.* **1965**, *42*, 288.
(49) Semenyuk, A. V.; Svergun, D. I. GNOM – a program package for small-angle scattering data processing. *J. Appl. Crystallogr.* **1991**, *24*, 537-540.
(50) Hammersley, A. P. FIT2D: a multi-purpose data reduction, analysis and visualization program. *J. Appl. Crystallogr.* **2016**, *49*, 646-652.

(51) Oliveira, C. L. P.; Vorup-Jensen, T.; Andersen, C. B. F.; Andersen, G. R.; Pedersen, J. S. Discovering new features of protein complexes structures by small-angle X-ray scattering. In *Applications of Synchrotron Light to Scattering and Diffraction in Materials and Life Sciences*, Gomez, M., Nogales, A., Garcia-Gutierrez, M. C., Ezquerra, T. A. Eds.; Springer Berlin Heidelberg, 2009; pp 231-244.
(52) Liz-Marzan, L. M. Gold nanoparticle research before and after the Brust–Schiffrin method. *Chem. Comm.* **2013**, *49*, 16-18.
(53) Brust, M.; Fink, J.; Bethell, D.; Schiffrin, D. J.; Kiely, C. Synthesis and reactions of functionalised gold nanoparticles. *Chem. Commun.* **1995**, 1655-1656.
(54) Brust, M.; Walker, M.; Bethell, D.; Schiffrin, D. J.; Whyman, R. Synthesis of thiol-derivatised gold nanoparticles in a two-phase liquid-liquid system. *Chem. Commun.* **1994**, 801-802.
(55) Perala, S. R. K.; Kumar, S. On the mechanism of metal nanoparticle synthesis in the Brust–Schiffrin method. *Langmuir* **2013**, *29*, 9863-9873.
(56) Ruks, T.; Loza, K.; Heggen, M.; Prymak, O.; Sehnem, A. L.; Oliveira, C. L. P.; Bayer, P.; Beuck, C.; Epple, M. Peptide-conjugated ultrasmall gold nanoparticles (2 nm) for selective protein targeting. *ACS Appl. Bio Mater.* **2021**, *4*, 945-965.
(57) Mahl, D.; Diendorf, J.; Meyer-Zaika, W.; Epple, M. Possibilities and limitations of different analytical methods for the size determination of a bimodal dispersion of metallic nanoparticles. *Coll. Surf. A* **2011**, *377*, 386-392.
(58) Amendola, V.; Pilot, R.; Frasconi, M.; Marago, O. M.; Iati, M. A. Surface plasmon resonance in gold nanoparticles: a review. *J. Phys. Condens. Matter* **2017**, *29*, 203002.
(59) Benfield, R. E.; Maydwell, A. P.; Ruitenbeek, J. M.; Leeuwen, D. A. Electronic spectra of metal cluster molecules. *Z. Phys. D* **1993**, *26* (S1), 4-7.
(60) Huang, Y. Y.; Fuksman, L.; Zheng, J. Luminescence mechanisms of ultrasmall gold nanoparticles. *Dalton Trans.* **2018**, *47*, 6267-6273.
(61) Fissan, H.; Ristig, S.; Kaminski, H.; Asbach, C.; Epple, M. Comparison of different characterization methods for nanoparticle dispersions before and after aerosolization. *Anal. Meth.* **2014**, *6*, 7324-7334.
(62) Wolff, N.; Kollenda, S.; Klein, K.; Loza, K.; Heggen, M.; Brochhagen, L.; Witzke, O.; Krawczyk, A.; Hilger, I.; Epple, M. Silencing of proinflammatory NF-κB and inhibition of herpes simplex virus (HSV) replication by ultrasmall gold nanoparticles (2 nm) conjugated with small-interfering RNA. *Nanoscale Adv.* **2022**, *4*, 4502-4516.
(63) Garcia, P. R. A. F.; Prymak, O.; Grasmik, V.; Pappert, K.; Wlysses, W.; Otubo, L.; Epple, M.; Oliveira, C. L. P. An in situ SAXS investigation of the formation of silver nanoparticles and bimetallic silver–gold nanoparticles in controlled wet-chemical reduction synthesis. *Nanoscale Adv.* **2019**, *2*, 225-238.
(64) Garcia, P. R. A. F.; Loza, K.; Daumann, S.; Grasmik, V.; Pappert, K.; Rostek, A.; Helmlinger, J.; Prymak, O.; Heggen, M.; Epple, M.; et al. Combining small-angle x-ray scattering and x-ray powder diffraction to investigate size, shape and crystallinity of silver, gold and alloyed silver-gold nanoparticles. *Braz. J. Phys.* **2019**, *49*, 183-190.
(65) Rostek, A.; Breisch, M.; Loza, K.; Garcia, P. R. A. F.; Oliveira, C. L. P.; Prymak, O.; Heggen, M.; Köller, M.; Sengstock, C.; Epple, M. Wet-chemical synthesis of Pd-Au core-shell nanoparticles (8 nm): From nanostructure to biological properties. *ChemistrySelect* **2018**, *3*, 4994-5001.
(66) Pedersen, J. S. Analysis of small-angle scattering data from colloids and polymer solutions: modeling and least-squares fitting. *Adv. Coll. Interface Sci.* **1997**, *70*, 171-210.
(67) Frolov, A. I.; Chankeshwara, S. V.; Abdulkarim, Z.; Ghiandoni, G. M. pIChemiSt — Free tool for the calculation of isoelectric points of modified peptides. *J. Chem. Inf. Model.* **2022**, *63*, 187-196.

(68) Salassa, G.; Burgi, T. NMR spectroscopy: A potent tool for studying monolayer-protected metal nanoclusters. *Nanoscale Horiz.* **2018**, *3*, 457-463.
(69) Salorinne, K.; Lahtinen, T.; Koivisto, J.; Kalenius, E.; Nissinen, M.; Pettersson, M.; Häkkinen, H. Nondestructive size determination of thiol-stabilized gold nanoclusters in solution by diffusion ordered NMR spectroscopy. *Anal. Chem.* **2013**, *85*, 3489-3492.
(70) Marbella, L. E.; Millstone, J. E. NMR techniques for noble metal nanoparticles. *Chem. Mater.* **2015**, *27*, 2721-2739.
(71) Wolff, N.; Loza, K.; Heggen, M.; Schaller, T.; Niemeyer, F.; Bayer, P.; Beuck, C.; Oliveira, C. L. P.; Prymak, O.; Weidenthaler, C.; et al. Ultrastructure and surface composition of glutathione-terminated ultrasmall silver, gold, platinum, and alloyed silver–platinum nanoparticles (2 nm). *Inorg. Chem.* **2023**, *62*, 17470-17485.
(72) Salorinne, K.; Malola, S.; Wong, O. A.; Rithner, C. D.; Chen, X.; Ackerson, C. J.; Häkkinen, H. Conformation and dynamics of the ligand shell of a water-soluble Au_{102} nanoparticle. *Nat. Comm.* **2016**, *7*, 10401.
(73) Dainese, T.; Agrachev, M.; Antonello, S.; Badocco, D.; Black, D. M.; Fortunelli, A.; Gascon, J. A.; Stener, M.; Venzo, A.; Whetten, R. L. Atomically precise Au144(SR)60 nanoclusters (R= Et, Pr) are capped by 12 distinct ligand types of 5-fold equivalence and display gigantic diastereotopic effects. *Chem. Sci.* **2018**, *9*, 8796-8805.
(74) Ruks, T.; Beuck, C.; Schaller, T.; Niemeyer, F.; Zähres, M.; Loza, K.; Heggen, M.; Hagemann, U.; Mayer, C.; Bayer, P.; et al. Solution NMR spectroscopy with isotope-labelled cysteine (^{13}C, ^{15}N) reveals the surface structure of L-cysteine-coated ultrasmall gold nanoparticles (1.8 nm). *Langmuir* **2019**, *35*, 767-778.
(75) Schuetze, B.; Mayer, C.; Loza, K.; Gocyla, M.; Heggen, M.; Epple, M. Conjugation of thiol-terminated molecules to ultrasmall 2 nm-gold nanoparticles leads to remarkably complex ^{1}H-NMR spectra. *J. Mater. Chem. B* **2016**, *4*, 2179-2189.
(76) Mingos, D. M. P. Gold Clusters, Colloids and Nanoparticles I. In *Structure and Bonding*, Springer: Heidelberg, 2014; Vol. 161.
(77) Rahme, K.; Chen, L.; Hobbs, R. G.; Morris, M. A.; O'Driscoll, C.; Holmes, J. D. PEGylated gold nanoparticles: polymer quantification as a function of PEG lengths and nanoparticle dimensions. *RSC Adv.* **2013**, *3*, 6085-6094.
(78) Picardi, G.; Humbert, B.; de la Chapelle, M. L.; Queffelec, C. Surface modification of Au nanoparticles with heteroleptic Cu(I) diimine complexes. *J. Phys. Chem. C* **2020**, *124*, 11902-11912.
(79) Ming, M.; Chen, Y.; Katz, A. Steady-state fluorescence-based investigation of the interaction between protected thiols and gold nanoparticles. *Langmuir* **2002**, *18*, 2413-2420.
(80) van der Meer, S. B.; Seiler, T.; Buchmann, C.; Partalidou, G.; Boden, S.; Loza, K.; Heggen, M.; Linders, J.; Prymak, O.; Oliveira, C. L. P.; et al. Controlling the surface functionalization of ultrasmall gold nanoparticles by sequence-defined macromolecules. *Chem. Eur. J.* **2021**, *27*, 1451-1464.
(81) Wetzel, O.; Prymak, O.; Loza, K.; Gumbiowski, N.; Heggen, M.; Bayer, P.; Beuck, C.; Weidenthaler, C.; Epple, M. Water-based synthesis of ultrasmall nanoparticles of platinum group metal oxides (1.8 nm). *Inorg. Chem.* **2022**, *61*, 5133-5147.
(82) Karki, I.; Wang, H.; Geise, N. R.; Wilson, B. W.; Lewis, J. P.; Gullion, T. Tripeptides on gold nanoparticles: structural differences between two reverse sequences as determined by solid-state NMR and DFT calculations. *J. Phys. Chem. B* **2015**, *119*, 11998-12006.
(83) Laibinis, P. E.; Whitesides, G. M.; Allara, D. L.; Tao, Y. T.; Parikh, A. N.; Nuzzo, R. G. Comparison of the structures and wetting properties of self-assembled monolayers of n-alkanethiols on the coinage metal surfaces, copper, silver, and gold. *J. Am. Chem. Soc.* **1991**, *113*, 7152-7167.

(84) Dubois, L. H.; Zegarski, B. R.; Nuzzo, R. G. Molecular ordering of organosulfur compounds on Au(111) and Au(100): Adsorption from solution and in ultrahigh vacuum. *J. Chem. Phys.* **1993**, *98*, 678-688.
(85) Chavez, M.; Sanchez-Obrero, G.; Madueno, R.; Sevilla, J. M.; Blazquez, M.; Pineda, T. Electrochemical evaluation of the grafting density of self-assembled monolayers of polyethylene glycol of different chain lengths formed by the grafting to approach under conditions close to the cloud point. *J. Electroanal. Chem.* **2022**, *913*, 116294.
(86) Wu, M.; Vartanian, A. M.; Chong, G.; Pandiakumar, A. K.; Hamers, R. J.; Hernandez, R.; Murphy, C. J. Solution NMR analysis of ligand environment in quaternary ammonium-terminated self-assembled monolayers on gold nanoparticles: the effect of surface curvature and ligand structure. *J. Am. Chem. Soc.* **2019**, *141*, 4316-4327.
(87) Hostetler, M. J.; Green, S. J.; Stokes, J. J.; Murray, R. W. Monolayers in three dimensions: synthesis and electrochemistry of ω-functionalized alkanethiolate-stabilized gold cluster compounds. *J. Am. Chem. Soc.* **1996**, 4212-4213.
(88) Hostetler, M. J.; Wingate, J. E.; Zhong, C. J.; Harris, J. E.; Vachet, R. W.; Clark, M. R.; Londono, J. D.; Green, S. J.; Stokes, J. J.; Wignall, G. D.; et al. Alkanethiolate gold cluster molecules with core diameters from 1.5 to 5.2 nm: core and monolayer properties as a function of core size. *Langmuir* **1998**, *14*, 17-30.
(89) Song, Y.; Harper, A. S.; Murray, R. W. Ligand heterogeneity on monolayer-protected gold clusters. *Langmuir* **2005**, *21*, 5492-5500.
(90) Rahnamoun, A.; Deline, A.; Zienkiewicz, J.; Bei, R. H.; Zheng, Z.; Rosenzweig, Z.; Fairbrother, D. H.; Hernandez, R. Surface curvature and aminated side-chain partitioning affect structure of poly(oxonorbornenes) attached to planar surfaces and nanoparticles of gold. *Langmuir* **2020**, *36*, 10412-10420.
(91) Lanterna, A. E.; Coronado, E. A.; Granados, A. M. When nanoparticle size and molecular geometry matter: Analyzing the degree of surface functionalization of gold nanoparticles with sulfur heterocyclic compounds. *J. Phys. Chem. C* **2012**, *116*, 6520-6529.
(92) Kenzler, S.; Fetzer, F.; Schrenk, C.; Pollard, N.; Frojd, A. R.; Clayborne, A. Z.; Schnepf, A. Synthesis and characterization of three multi-shell metalloid gold clusters Au32(R3P)12Cl8. *Angew. Chem. Int. Ed. Engl.* **2019**, *58*, 5902-5905.
(93) Schnoeckel, H.; Schnepf, A.; Whetten, R. L.; Schenk, C.; Henke, P. A chemical view of the giant Au-102(SR)(44) (SR = p-mercaptobenzoic acid) cluster: Metalloid aluminum and gallium clusters as path making examples of this novel type open our eyes for structure and bonding of metalloid Au-n(SR)(m) (n > m) clusters. *Z. Anorg. Allg. Chem.* **2011**, *637*, 15-23.
(94) Jadzinsky, P. D.; Calero, G.; Ackerson, C. J.; Bushnell, D. A.; Kornberg, R. D. Structure of a thiol monolayer-protected gold nanoparticle at 1.1 Å resolution. *Science* **2007**, *318*, 430-433.
(95) Sokolova, V.; Ebel, J. F.; Kollenda, S.; Klein, K.; Kruse, B.; Veltkamp, C.; Lange, C. M.; Westendorf, A. M.; Epple, M. Uptake of functional ultrasmall gold nanoparticles in 3D gut cell models. *Small* **2022**, *18*, 2201167.
(96) van der Meer, S. B.; Loza, K.; Wey, K.; Heggen, M.; Beuck, C.; Bayer, P.; Epple, M. Click chemistry on the surface of ultrasmall gold nanoparticles (2 nm) for covalent ligand attachment followed by NMR spectroscopy. *Langmuir* **2019**, *35*, 7191-7204.
(97) Stahl, P.; Kollenda, S.; Sager, J.; Schmidt, L.; Schroer, M. A.; Stauber, R. H.; Epple, M.; Knauer, S. K. Tuning nanobodies' bioactivity: Coupling to ultrasmall gold nanoparticles allows the intracellular interference with survivin. *Small* **2023**, *13*, 2300871
(98) Ha, J. M.; Soloyyov, A.; Katz, A. Accessibility in calix 8 arene-bound gold nanoparticles: crucial role of induced-fit binding. *J. Phys. Chem. C* **2010**, *114*, 16060-16070.
(99) Rai, A.; Pinto, S.; Velho, T.; Ferreira, A. F.; Moita, C.; Trivedi, U.; Evangelista, M.; Comune, M.; Rumbaugh, K. P.; Simoes, P. N.; et al. One-step synthesis of high-density

peptide-conjugated gold nanoparticles with antimicrobial efficacy in a systemic infection model. *Biomaterials* **2016**, *85*, 99-110.
(100) Li, Y.; Juarez-Mosqueda, R.; Song, Y.; Zhang, Y.; Chai, J.; Mpourmpakis, G.; Jin, R. Ligand exchange on Au-38(SR)(24): substituent site effects of aromatic thiols. *Nanoscale* **2020**, *12*, 9423-9429.
(101) Salassa, G.; Sels, A.; Mancin, F.; Burgi, T. Dynamic nature of thiolate monolayer in Au-25(SR)(18) nanoclusters. *ACS Nano* **2017**, *11*, 12609-12614.
(102) Fisher, A. A. E.; Osborne, M. A.; Day, I. J.; Lucena Alcalde, G. Measurement of ligand coverage on cadmium selenide nanocrystals and its influence on dielectric dependent photoluminescence intermittency. *Commun. Chem.* **2019**, *2*, 63.
(103) Wetzel, O.; Hosseini, S.; Loza, K.; Heggen, M.; Prymak, O.; Bayer, P.; Beuck, C.; Schaller, T.; Niemeyer, F.; Weidenthaler, C.; et al. Metal–ligand interface and internal structure of ultrasmall silver nanoparticles (2 nm). *J. Phys. Chem. B* **2021**, *125*, 5645-5659.
(104) Ruks, T.; Loza, K.; Heggen, M.; Ottmann, C.; Bayer, P.; Beuck, C.; Epple, M. Targeting the surface of the protein 14-3-3 by ultrasmall gold nanoparticles (1.5 nm), carrying the specific peptide CRaf. *ChemBioChem* **2021**, *22*, 1456-1463.
(105) Rostek, A.; Mahl, D.; Epple, M. Chemical composition of surface-functionalized gold nanoparticles. *J. Nanopart. Res.* **2011**, *13*, 4809-4814.

TOC Graphic

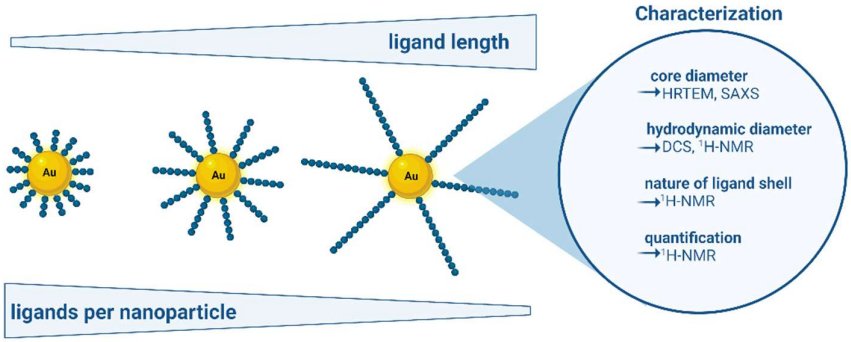
ligand length
Au
Au
Au
ligands per nanoparticle
Characterization
core diameter
→HRTEM, SAXS
hydrodynamic diameter
→DCS, ^{1}H-NMR
nature of ligand shell
→^{1}H-NMR
quantification
→^{1}H-NMR